

E-WASTE MANAGEMENT IN THE SEMICONDUCTOR INDUSTRY

by

AUTHOR NAME

A master's thesis submitted to the Graduate Faculty in Liberal Studies in partial
fulfillment of the requirements for the degree of Master of Science,
The City University of New York

2025

© 2025

AUTHOR NAME

All Rights Reserved

E-WASTE MANAGEMENT IN THE SEMICONDUCTOR INDUSTRY:

by

AUTHOR NAME

This manuscript has been read and accepted for the Graduate Faculty in
Liberal Studies in satisfaction of the thesis requirement
for the degree of Master of Science.

Approved:

Faculty Name, Advisor

Faculty Name, Executive Officer

THE CITY UNIVERSITY OF NEW YORK

E-WASTE MANAGEMENT IN THE SEMICONDUCTOR INDUSTRY:

by

AUTHOR NAME

Advisor: Faculty name

The semiconductor industry is central to global technology development, powering everything from mobile phones and computers to automobiles and medical devices. As chips become smaller and more complex, semiconductor manufacturers generate significant byproducts and end-of-life electronic devices that require specialized handling. Globally, an estimated 57.4 million metric tons (Mt) of e-waste were produced in 2021. Since data on e-waste began to be gathered in 2014, the number has increased annually. Current statistics show that only 17.4% of global e-waste is recycled through formal channels, and this figure is likely even lower for specialized semiconductor waste streams due to their complexity. Furthermore, semiconductor manufacturing involves hazardous materials, like arsenic, gallium, and various doping chemicals, that need meticulous management. Without proper disposal or recycling, such wastes contribute to air, water, and soil pollution, posing health hazards. Consequently, the semiconductor industry needs comprehensive, automated, and safe recycling technologies that minimize environmental impact while recovering valuable metals and critical materials, such as silicon, rare earths, and gold. The proposed research will leverage advanced Artificial Intelligence (AI) solutions to optimize the e-waste management cycle. It will address specialized e-waste streams from chip manufacturing, assembly, and consumer electronics containing semiconductor components..

CONTENTS

List of Figures	2
List of Tables	3
CHAPTER I	5
1. INTRODUCTION	5
1.1. Motivation	5
1.2. Global E Waste Overview	5
1.3. Focus on PCB's	6
1.4. Small Dataset Problem	6
1.5. Thesis Organization	7
CHAPTER II	8
2. LITERATURE REVIEW	8
2.1. Previous Work	8
2.2. Hazardous Materials	9
2.3. Current Approaches to E-Waste Recycling	12
2.4. Emerging Technologies	13
2.5. Gaps in Research	16
CHAPTER III	17
3. METHODOLOGY	17
3.1. Physical datasets available	17
3.2. Introduction to dataset	27
3.3. Methodologies	29
3.4. Evaluation Metrics	40
3.4. Proposed Approach	42
CHAPTER IV	43
4. RESULTS AND ANALYSIS	43
4.1. Model Performance	54
4.2. Comparative Analysis	57
4.3. Result Analysis	54
4.4. Classification models	62
CHAPTER V	68
5. CONCLUSION	68

LIST OF FIGURES

FIGURE NO

Fig 1. Sample Dataset images.....	17
Fig 2. Sample detection images using YOLO11.....	18
Fig 3. Sample Defect image and its detection image.....	19
Fig 4. Detection images using PCBA-DET Dataset.....	20
Fig 5. sample image and the respective masks including General and Monoseg Mask images..	20
Fig 6. Predicted mask of sample image using UNET.....	21
Fig 7. sample image and the Performance on PCB-METAL using Retinanet-50 from dataset..	22
Fig 8. Sample image, annotated and detection results using YOLO from dataset.....	23
Fig 9. FPIC component dataset with 768X768 patch sample.....	24
Fig 10. Sample original image and the ground truth image.....	25
Fig 11 . Sample DeepPCB image with its annotated image.....	26
Fig 12. Sample FICS PCB images (8256x5504) with its gt-masks.....	28
Fig 13: sample augmentation examples for the FICS-PCB dataset.....	36
Fig 14 . Chart displaying class distribution of segmentation.....	37
Fig 15: Sample extracted patches (1024×1024 crops resized to 640×640).....	43
Fig 16. Segmentation Results for PCB-VISION with WCCE loss function.....	44
Fig 17. Segmentation Results for FICS-PCB with WCCE loss function.....	45
Fig 18: Predicted Masks using Hybrid loss function.....	48
Fig 19. Predicted Masks overlays.....	50
Fig 20. Predicted Masks using FICS-PCB.....	52
Fig 21. Predicted Masks overlays.....	54
Fig 22. Class-wise DICE and IOU metrics graphs for FICS-PCB images.....	61
Fig 23. labeled FICS-PCB components from the dataset.....	62
Fig 24. FPIC-PCB class composition.....	62
Fig 25. Classification results on FICS-PCB using many recent popular DL models.....	66
Fig 26. Sample misclassified classes.....	66

LIST OF TABLES

FIGURE NO

Table 1. Some of the common Toxic Substances found in E waste and its impact on Health.....	10
Table 2. Existing methods to E-waste Recycling and its Limitations.....	12
Table 3. Recent AI approaches on PCB images focusing on different datasets and metrics.....	14
Table 4 : Summary of existing datasets.....	26
Table 5: Component Analysis in an image (FICS-PCB).....	28
Table 6: Summary of the augmentations applied on the dataset.....	34
Table 7: Class distribution based on pixel counts FICS-PCB.....	37
Table 8: Model Config for training the segmentation model.....	38
Table 9: Segmentation results using Pre Training on PCB-VISION dataset.....	54
Table 10: Segmentation results without using Pre Training on PCB-VISION dataset.....	55
Table 11: Segmentation results using Pre Training on FICS-PCB dataset.....	55
Table 12: Segmentation results without using Pre Training on FICS-PCB dataset.....	56
Table 13: Comparison of Classification Results.....	64
Table 14: Comparison of Class wise F1-Scores on FICS-PCB dataset.....	64

Digital Manifest

1. Git Repository containing the thesis PCB Segmentation and Classification Files including notebooks outputs and models networks used. More information is detailed in the readme file on the github.

Url: <https://github.com/tejasai777/PCB-Component-SegClass-Networks-pytorch>

INTRODUCTION

1.1. Motivation

The rapid expansion of the semiconductor industry has drastically amplified the generation of electronic waste (e-waste), particularly from printed circuit boards (PCBs) containing complex semiconductor components. Efficient e-waste management is not merely an environmental imperative but also an economic opportunity, as vast amounts of high-value raw materials remain unrecovered. This thesis aims to address the urgent need for targeted solutions to manage and recycle semiconductor-specific e-waste.

1.2. Global E-Waste Overview

E-waste is among the fastest-growing waste streams globally, with an estimated 62 million tonnes [1] generated in 2022. Alarmingly, only 22.3% [2] was formally collected and recycled, leaving a significant portion unaccounted for. Informal e-waste recycling activities exacerbate environmental and health concerns, releasing hazardous substances like lead into the environment. Children and pregnant women are particularly vulnerable to these adverse effects (World Health Organization. (2024) [2]. Additionally, greenhouse gases released from improperly handled e-waste contribute to climate change.

E-waste contains valuable materials such as gold, silver, copper, and palladium. For instance, recycling one million used mobile phones can recover approximately 75 lbs of gold, 772 lbs of silver, and 35,000 lbs of copper [3]. The economic loss due to unrecycled materials is significant, with the 53.6 Mt of e-waste generated in 2019 containing an estimated \$57 billion worth of

recoverable raw materials, of which \$47 billion went unrecovered [4]. With the global e-waste management market projected to grow from \$49,880 million in 2020 to \$143,870 million by 2028, (Ruiz, A. (2024) addressing this challenge is a pressing economic and environmental necessity [5 , 7].

1.3. Focus on PCBs

Printed circuit boards(PCB's) are a primary source of semiconductor-specific e-waste. They contain hazardous materials like arsenic, gallium, and rare earths, alongside high-value metals [6]. The complexity and heterogeneity of PCBs make traditional recycling methods inefficient. End-of-life electronic devices (e.g., smartphones, laptops, IoT devices) which are discarded over the use or once damaged and manufacturing byproducts such as defective chips and chemical residues further contribute to the challenges of PCB waste management. Early research [8] highlighted the economic potential of recovering precious metals but lacked a specific focus on specialized semiconductor waste.In recent studies it is noted that semiconductor-specific recycling rates are likely lower than the global e-waste recycling average of 17.4% [9], emphasizing the need for tailored approaches. There is a lot of research and applications available on e waste recycling using visual intelligence but very little research is done in specialised e waste recycling focusing specifically on PCBs and will discuss the reason behind it in our next section.

1.4. Small Dataset Problem

A critical challenge in PCB e-waste research is the availability of small, specialized datasets for training AI models [10 , 11]. Also another reason is the diverse range of electronic waste and the

cost involved in annotating all the components from all the components. This issue hinders the development and validation of innovative technologies for efficient PCB component segmentation and classification, which are vital for recycling. However there is rapid improvement in many state of the art techniques that can be applied to address this issue and achieve good results detecting many components even with fewer PCB data.

1.5. Thesis Organization

The structure of the thesis is organized as follows:

In Chapter 2 ,a literature Review on e-waste management, focusing on hazardous materials, current recycling approaches, and emerging technologies.

Chapter 3 outlines the proposed methodology, dataset used in the study as well as architectures , Listing of 25 components mainly of PCBs that are significant in e waste recycling in the semiconductor industry, we also discuss model training, and evaluation metrics.

Chapter 4 focuses on the results and analysis from this project, including model performance, visual outputs, and a comparative analysis of approaches.

Chapter 5 encompasses the conclusions drawn from this study and suggests future research directions.

LITERATURE REVIEW

2.1. Previous Work

There have been several recent emerging studies using custom datasets and some experiments on publicly available datasets particularly in PCBs. However most do not focus on e-waste management . The first study by Muhammad Mohsin et al. (2025) discusses the effectiveness of multiple variants of YOLO models (v8, v9, v10, v11) using custom WPCB images dataset , achieving an impressive average precision of 99.8% and F1-score of 99.5% [\[12\]](#). However, their approach was limited to common components and required specialized hardware.

The second recent study by Matko Glucina et al. (2023) explored using Micro-pcb Images Dataset [\[14\]](#) with a YOLOv5 architecture, achieving a F1 score above 0.99 [\[15\]](#)for segmentation . While this method looks promising, its reliance on the undamaged Microcontroller images data may not fully translate to real-world PCB image components detection ; however their future scope suggests a work on real time image dataset of PCB images.

The third one is a thesis defense by Khan et al. (2024) at Kansas University discusses and compared various models including Enhanced U-Net, SAM, and Detectron2+ResNeXt-101 on the FPIC Dataset, achieving 97.08% DICE and 96.34% accuracy [\[16\]](#). However, their study was limited to only five component types and faced some computational complexity challenges.

The fourth study by Minghui Shen et al. (2024) introduced PCBA-YOLO, a YOLOv5 variant, which achieved a 97.3% mAP [\[17\]](#) on the PCBA-DET dataset. While this is effective,

this approach focused primarily on assembly defects rather than recycling applications and it requires diverse data to detect defects precisely.

Jessurun, N et al. (2021) study discusses comparison of neural networks for PCB component segmentation using models U-Net, DilatedNet, DeepLab, LinkNet, ICNet on the dataset consisted of RGB images of SMDs that belonged to one of 5 classes: resistor, capacitor, transistor, inductor, and integrated circuit (IC),, where it achieved an impressive scores of 0.96 Dice Coefficient and 0.96 accuracy score [\[20\]](#), but, this method faces challenges with limitation of images and addresses the future on larger dataset.

Most recently, Elias Arbash et al. (2024) utilized various U-Net architectures using custom made PCB-Vision dataset [\[19\]](#), achieving high precision of 0.98 and 0.97 using AttentionUNet and U-Net [\[18\]](#) on HSI patches and more. However, their small dataset of 53 images and challenges in HSI processing limit broader applicability.

Despite the variety in custom datasets, including both labeled and unlabeled ones, many approaches rely on expensive computational resources and custom models, limiting their scalability . This study addresses these challenges by leveraging well-annotated PCB datasets with more classes and advanced state-of-the-art models that can be computationally efficient and effective even for dense and small-component PCB datasets for a specialised e-waste recycling approach.

2.2. Hazardous Materials

Semiconductor manufacturing involves hazardous materials such as arsenic, gallium, lead, and doping chemicals, which pose significant environmental and health risks if not

managed properly [24, 25]. These materials are often embedded in complex matrices within electronic components, making their extraction and disposal challenging.

For example, gallium arsenide (GaAs) used in high-frequency chips is highly toxic and requires specialized recycling processes , especially Arsenic which is highly dangerous affecting breathing and liver diseases and also causes bladder cancer as mentioned in the book published by (Rowan Cabrera (2020)) [21] including Arsine poisoning. In another research by (Chalana, A. et al. (2023)) on toxic metals it was mentioned that high levels of Ni (0.4%), Pb (1.5%), Zn (2.1%), Ba (0.3%), and Cd (310 mg/kg) are present in the soil samples from CRT storage sites. The concentration of lead in these soil samples was 50 times more (1580 mg/kg) than the background soil concentration (30 mg/kg) which is to be concerned [22, 27].

The presence of rare earth elements (REEs) and precious metals, such as gold and silver, further complicates recycling efforts due to their economic value and environmental impact if improperly handled (Hema Jha (2024)). Efficient and cost-effective recycling methods are essential to mitigate these risks and recover valuable materials. A critical step in this process is the segmentation of hazardous components before they are incinerated or disposed of, as improper handling can lead to severe environmental hazards [23].

Table 1. Some of the common Toxic Substances found in E waste and its impact on Health

Toxic Metal	Source	Impact on Health	Reference
Lead (Pb)	Solder, semiconductor chips,PCBs	Skin damage, headache, nausea, gastric and duodenal ulcers, damage blood, brain, and nervous system in adult	Pourya, Z et al. (2023) [24, 25] and Patwa, J. et al. (2022) [27]

Mercury (Hg)	Switch relays, Fluorescent lamps in PCBs	Effect brain, Liver kidney, and central nervous system	Omondi, E. et al. (2022) [25] , Nyeko, S et al. (2023) [28]
Cadmium (Cd)	Semiconductor chips, Rechargeable Batteries	Respiratory system, kidney, bone problem, carcinogenic and defect in neurodevelopment of fetus	Abdelbasir, S. et al. (2018) [26] and Patwa, J. et al. (2022) [27]
Arsenic (As)	Doping agent in semiconductors and LEDs	Affect breathing, cardiovascular diseases, increase the risk of bladder cancer, gastrointestinal disturbances, liver and renal disease	Patwa, J. et al. (2022) [27]
Nickel (Ni)	Batteries, PCBs,Cathode ray tubes	Vomiting, diarrhoea, convulsions, coma or even death	Nyeko, S et al. (2023) [28]
Lithium (Li)	Batteries, PCBs,Cathode ray tubes	Affect gastrointestinal and long exposure leads to cancer	Nyeko, S et al. (2023) [28]
BFRs,PBDEs,TBBPA	Flame Retardants in PCBs, Keyboards,Plastic Casings	During combustion, printed circuit boards and plastic housings emit toxic vapors known to cause hormonal disorders	Charitopoulou et al. (2021) [29]
Persistent Organic Pollutants (POPs)	Printed Circuit boards(PCBs)	Immune system suppression, neurodevelopmental issues, and cancer (e.g., liver, skin).	Habib (2016), Leung, A. O. W. (2019). [30]

2.3. Current Approaches to E-Waste Recycling

Current e-waste recycling processes include Manually dismantling and sorting, chemical recycling, and thermal processes, such as leaching using liquids like acids mentioned in (Barrueto, Y et al (2022)) [\[31\]](#), Bioremediation uses microorganisms to degrade or extract pollutants and this is discussed in research by (Li, X. et al (2022)) [\[32\]](#), hydrometallurgy, uses solvents to extract metals but generates hazardous byproducts. Thermal methods, including pyrolysis used in WPCB recycling (Yunfeng Zhu et al. (2023))[\[33\]](#) and smelting, are effective for metal recovery but are energy-intensive and emit toxic gases . with each having its limitations in their process where it involves manpower, high end resources, and lack of precision considering recent developments in the semiconductor industry which is focused on smaller size components and circuit boards. Mechanical recycling involves shredding and sorting e-waste but this method struggles with the fine separation of semiconductor components.

Table 2. Existing methods to E-waste Recycling and its Limitations

Year	Method	Paper Source	Limitations
2024	Manual Dismantling	López, M. et al. [41]	Informal recycling practices release heavy metals and POPs into the environment.
2022	Thermal Plasma coupled with acid leaching	(Barrueto, Y et al (2022)) [31]	Issues with slag formation and emission control during pyrometallurgical processes.
2023	Physical and Chemical Process	Wang, Kaiqi. [34]	Technical and environmental limitations in recovering REEs.
2019	Automated Sorting Using Sensors	R. Laszlo et al. [35]	Economic feasibility and regulatory gaps hinder widespread adoption.

2024	Manual Sorting and Chemical, Thermal Techniques	Oke, E.A. et al. [40]	High initial costs and complexity in handling diverse e-waste materials.
2022	Pyrometallurgy	Faraji, F et al. [39]	Presence of flame retardants in plastics complicates recycling.
2019	Hydrometallurgical Processing	Ahamed Ashiq et al. [36]	Economic and environmental challenges in large-scale application.
2021	Bioremediation	M. Narayanasamy et al. [37]	Limited scalability and efficiency in treating complex e-waste streams.
2022	Phytoremediation	Haochen Yu et al. [38]	Limited to specific contaminants and requires long treatment times.

While these approaches are useful and traditional they require use of a lot of manpower,hazardous chemicals , Operational Costs and considering the variability in PCBs where size of the components are gradually decreasing in structure it is not an efficient way to do manual, Chemical ,thermal procedures for recycling. AI-driven approaches, such as state-of-the-art deep learning models, have improved the precision of e-waste disassembly and sorting but often require well-annotated datasets and significant computational resources. While a variety of datasets are available, including both labeled and unlabeled ones, the process of annotating PCB components is laborious and costly. Our current work focuses on taking advantage of AI models that will achieve optimal performance while maintaining computational efficiency, even for dense and small-component PCB datasets.

2.4. Emerging Technologies

Emerging technologies in e-waste management focus on improving efficiency, scalability, and environmental sustainability. AI-driven solutions, such as computer vision and robotic disassembly, are gaining traction for their ability to automate the identification and sorting of e-waste components. However, many of these methods rely on custom models and expensive computational resources, limiting their practicality for large-scale applications. Recent advancements in lightweight deep learning models and edge computing offer more efficient alternatives for real-time applications. Additionally, bioleaching and closed-loop recycling systems provide environmentally friendly methods for metal recovery. Despite these innovations, there is a need for cost-effective and scalable solutions tailored to the semiconductor industry, compared to current extreme computationally expensive approaches which our study aims to address

Table 3. Recent AI approaches on PCB images focusing on different datasets and metrics

Authors & Year	Dataset	Models/Met hods	Metrics	Performance	Limitations
Muhammad Mohsin et al. (2025) [12]	Custom WPCB images of V-PCB dataset [12]	Different YOLO models(v8,v9 ,v10,v11)	Inference time, Average Precision ,recall ,f1 score	Average Precision 99.8% and F1-score 99.5% [12]	Limited to common components, requires specialized hardware
Matko Glucina et al. (2023) [15]	Micro-pcb Images Dataset [14]	YOLOv5	F1-Score	>0.99 segmentation accuracy [15]	Limited Data and reliance of undamaged pcb images, no component detection
Khan et al. (2024) [16]	FPIC Dataset [42]	1. Enhanced U-Net	DICE, IoU, Accuracy	97.08% DICE,	Limited to 5 component

		2. SAM 3.Detectron2 +ResNeXt-101		96.34% accuracy [16]	types, computational complexity
Minghui Shen et al. (2024) [17]	PCBA-DET [17], [Baidu]	PCBA-YOLO (YOLOv5 variant)	mAP, Loss values	97.3% mAP [17]	Focused on assembly defects, not recycling
Elias Arbash et al. (2024) [18]	PCB-Vision (RGB-HSI) [19]	Unet, AttentionUnet, ResUnet and more	Precision, Recall, F1 Score, IOU	High precision of 0.98 and 0.97 using AttentionUnet and Unet on HSI patches test set [18]	Small dataset (53 images), HSI processing challenges
Jessurun, N et al. (2021) [20]	RGB images of SMDs [20]	U-Net, DilatedNet, DeepLab, LinkNet, ICNet	Dice Score ,f1 score	0.96 Dice Coefficient and 0.96 accuracy score [20]	limitation of images and addresses the future on larger dataset.
Liu, L et al.(2023) [43]	Laboratory-built PCB images of 1458 sheets(128x128 sizes) [43]	Mobile-Deep Others: UNet, PSPNet, DeepLab, PCBSegClassNet,	Precision, Recall, F1-score, mIoU	Segmentation results of Mobile-Deep Network with 94.87 precision, 93.64 F1-score [43]	Limited to only pcb images under laboratory environment performs poor with real world data. (Pcb defect detection)
Makwana, D et al..(2022) [44]	FPIC Component [45]	PCBSegClassNet Others: UNet, DeepLab, Swin Transformer, PVT-small,	DICE, IoU, ModelSize	(5.58mb) light weight model with DICE 96.29, IoU 92.7 score [44]	Hardware constraints, relies heavily on quality and diversity of training data

2.5. Gaps In Research

While significant progress has been made in e-waste management, several gaps remain, particularly in the context of dataset availability, computational efficiency, and cost-effectiveness. Existing methods often rely on custom models and extremely computational powerful methods and resources, making them impractical for large-scale deployment (For example despite its higher performance results models such as the DETR which requires High end GPUs and huge training hours is not computationally efficient for large scale applications) . Additionally, the process of annotating PCB components is laborious and costly, limiting the availability of well-annotated datasets. Lightweight models and edge computing solutions have been proposed but often focused on limited components and some lack efficiency.

Our work bridges the gap by leveraging a well-annotated PCB dataset with more important classes and using methods leveraging state of the art models that are computationally efficient and effective even for dense and small-component PCB datasets. Our main goal is to provide an optimal method for specialized e-waste management in the semiconductor industry. This is particularly important, where scalable and sustainable recycling solutions are a critical need .

METHODOLOGY

3.1. Physical Datasets Available:

WPCB

The dataset was acquired using an Arducam 12.4 MP camera which is connected to an NVIDIA Jetson Nano under diverse recycling conditions. The images taken consider the conditions such as variations in lighting, orientations, distances from the camera, cast shadows, viewpoints, and also resolutions. The dataset consists of high-resolution images of Waste Printed Circuit Boards shortly known as WPCBs, where all images are annotated with labeled components such as capacitors, integrated circuits (ICs), electrolytic capacitors, resistors, diodes, transistors, coils, and transformers.

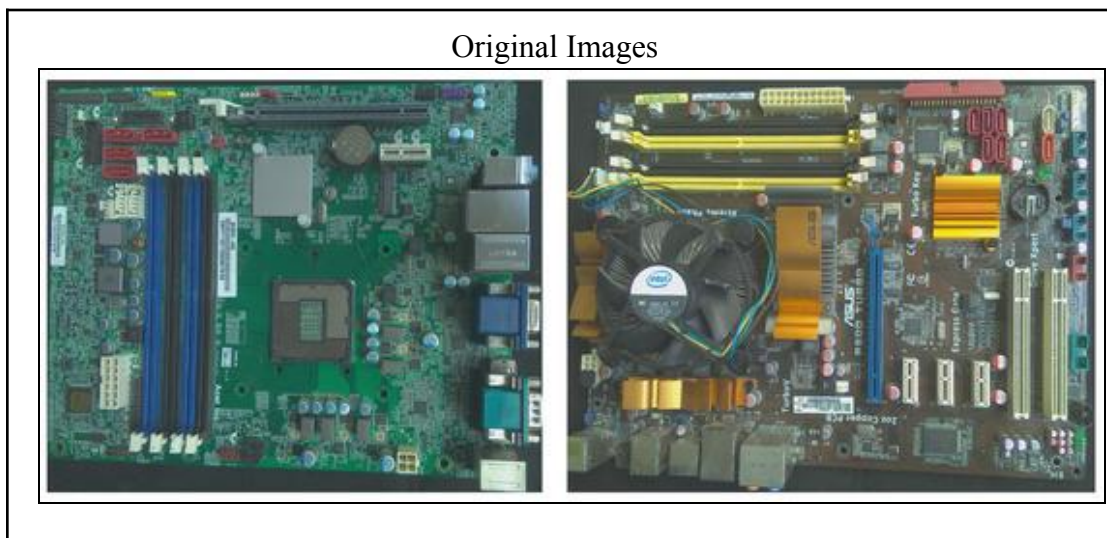


Fig 1. Sample Dataset images[\[12\]](#)

Muhammad Mohsin et al. (2025)[\[12\]](#) utilised this dataset with multiple variants of YOLO models (v8, v9, v10, v11) , achieving an impressive average precision of 99.8% and F1-score of 99.5% [\[12\]](#) . It is also noticed to have better performance of detection with yolov11 at

high-resolution images 1920×1920 few results of detection were also shown below with the sample images.

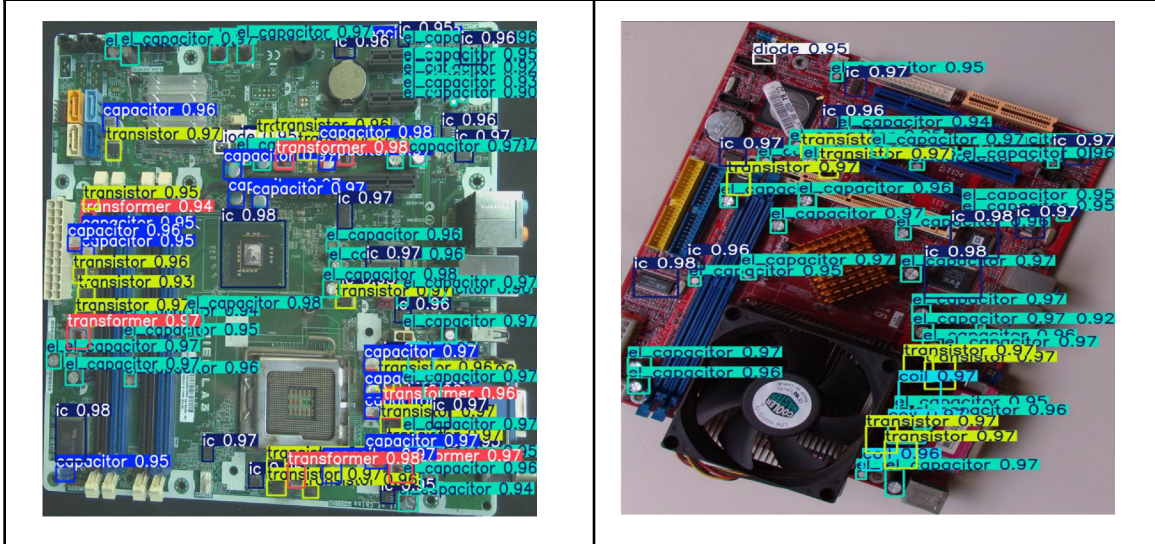


Fig 2. Sample detection images using YOLO11[12]

PCBA-defect

The PCBA-Defect dataset was custom created by capturing high-resolution images with a resolution of 4608×3456 pixels for PCB template boards using a 16-megapixel industrial camera also equipped with adjustable zoom lenses and optimized LED lighting to reduce distortions and shadows[47]. The images are annotated with labels of six defect types such as missing hole, mouse bite, open circuit, short circuit, spur, and spurious copper which were manually introduced using Photoshop. Each defect is annotated with bounding boxes and its coordinates pointing defect location. To simulate the real-world conditions and support algorithm evaluation for inspection processes, the images were captured in various orientations for better performance in defect detection[47].

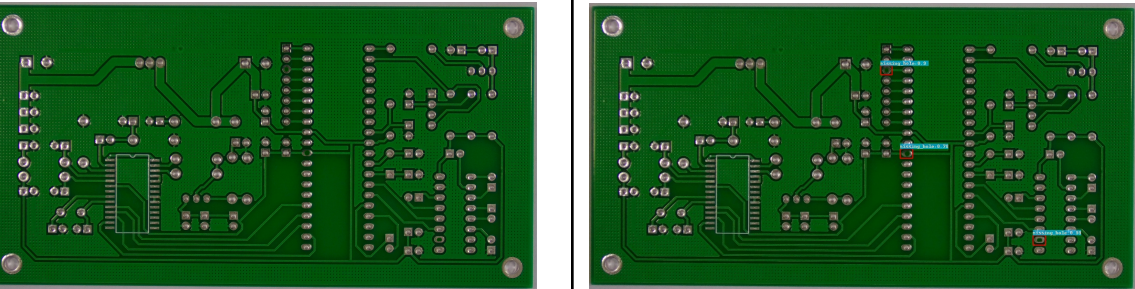


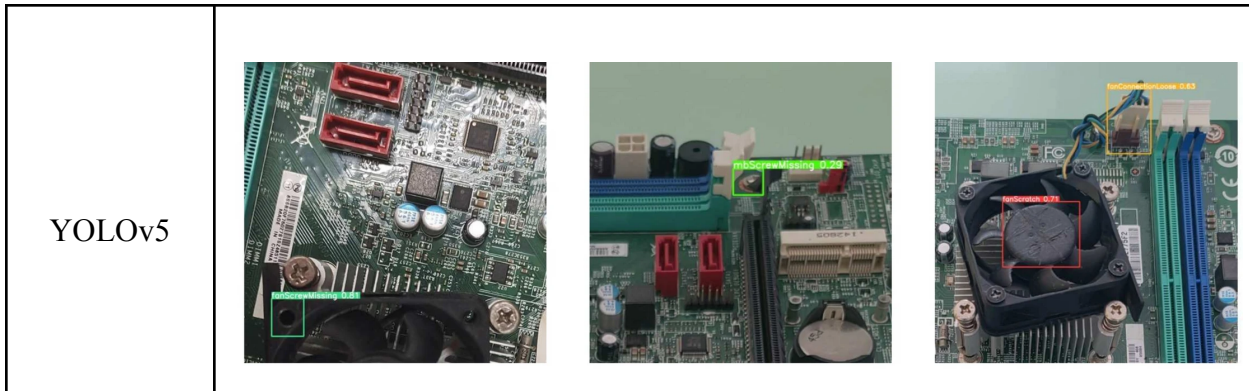
Fig 3. sample Defect image and its detection image [18],

PCBA-DET

The PCBA-DET dataset consists of 4000 images of PCBAs manually photographed from various angles to mimic real-world manufacturing pipelines. It includes 18,100 labeled defects including 8 classes, with annotations formatted in YOLO txt files describing its defect type and bounding box coordinates [17].

Minghui Shen et al. (2024) introduced PCBA-DET, a YOLOv5 variant achieving 97.3% mAP [17], However it focuses on detecting assembly defects rather than recycling applications.

Below are the sample results of the detection using PCBA-DET and YOLOv5 to compare



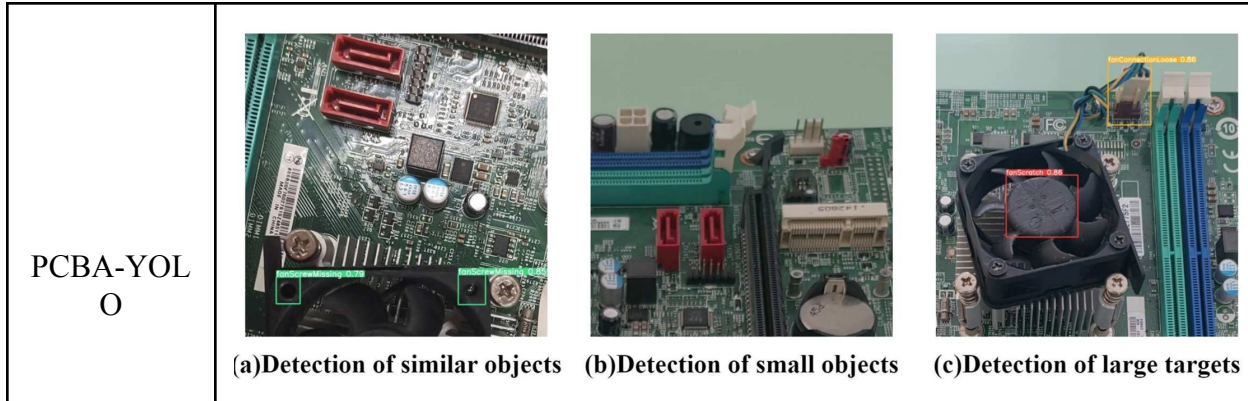


Fig 4. Detection images using PCBA-DET Dataset [17]

PCB-Vision

The PCB-Vision dataset includes 53 Printed Circuit Boards (PCBs) captured in RGB format using a Teledyne Dalsa C4020 camera on a conveyor belt and hyperspectral images (HSI) captured using a Specim FX10 spectrometer. The HSI data spans 224 bands within the VNIR range (400–1000 nm)[19]. Masks are provided for segmentation tasks with up to three classes: Others (0), IC (1), Capacitors (2), and Connectors (3). However, these classes are not balanced, object-wise and pixel-wise across the dataset. These masks are available in both 'General' and 'Monoseg' formats for segmentation analysis.

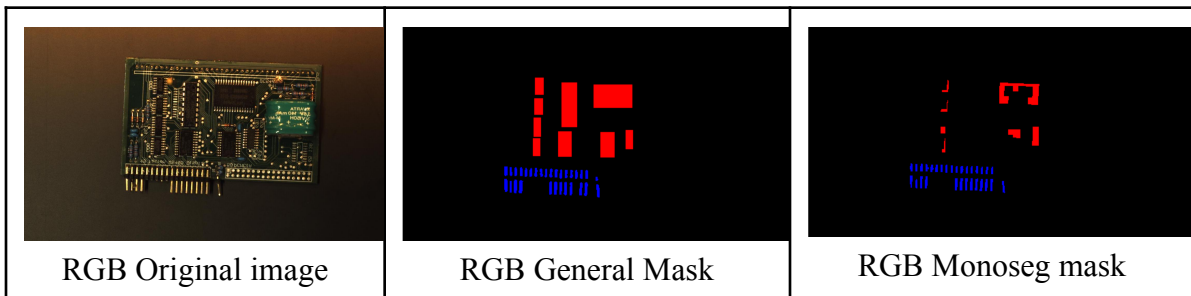


Fig 5. sample image and the respective masks including General and Monoseg Mask images[19]

Elias Arbash et al. (2024) achieved a high precision (0.97/0.98)[19] with Unet and AttentionUNet on a small PCB-Vision dataset (53 images), utilizing RGB-HSI processing

despite its challenges[19]. Below is a sample image with predicted and ground truth mask using UNET model.

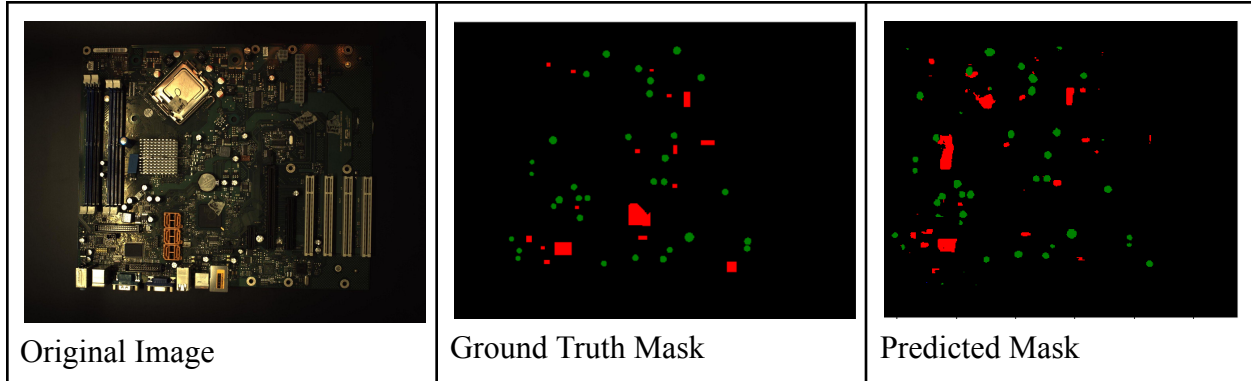


Fig 6. Predicted mask of sample image using UNET [19]

PCB-Metal

The PCB-Metal dataset consists of high-resolution PCB images that are captured using a Canon EOS 5D Mark II DSLR camera under professional lighting conditions ensuring consistent image quality. It includes bounding box annotations for 5,844 IC chips, 3,175 capacitors, 2,679 resistors, and 542 inductors across 123 pcb boards at varying rotations of 0°, 90°, 180°, and 270°[49]. These annotations help automated systems for component detection and reverse engineering processes that are traditionally manual. Additionally Baseline evaluations of deep learning-based object detection techniques are also included to demonstrate their effectiveness in detecting the IC chips.

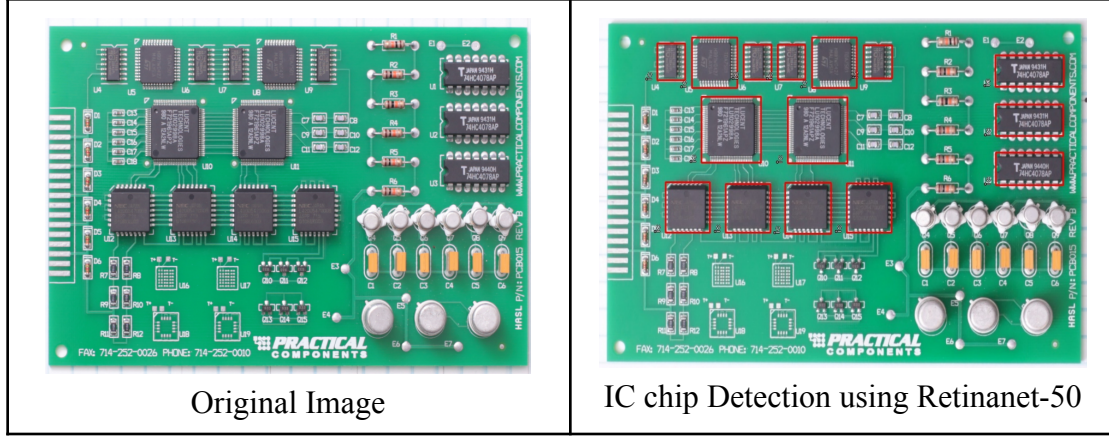


Fig 7. sample image and the Performance on PCB-METAL using Retinanet-50 from dataset[\[49\]](#)

PCB-DSLR

The PCB-DSLR dataset provides high-resolution images (4928×3280 pixels at 222ppi) of 165 PCBs that are captured using a Nikon D4 DSLR camera with a 60mm f/2.8 lens mounted above a black conveyor belt to simulate real-world recycling conditions[\[50\]](#). Also under conditions with controlled illumination with polarized light and opaque curtains minimizes reflections. Each PCB is represented by 3–5 images taken from varying orientations and positions resulting in precise detection of components under varying angles as there are plenty of PCB layers organized differently . The dataset includes segmentation information, bounding box annotations for 9,313 IC chips, and textual data for 1,740 chips supporting applications such as automatic segmentation, component detection, and text recognition in recycling processes[\[50\]](#).

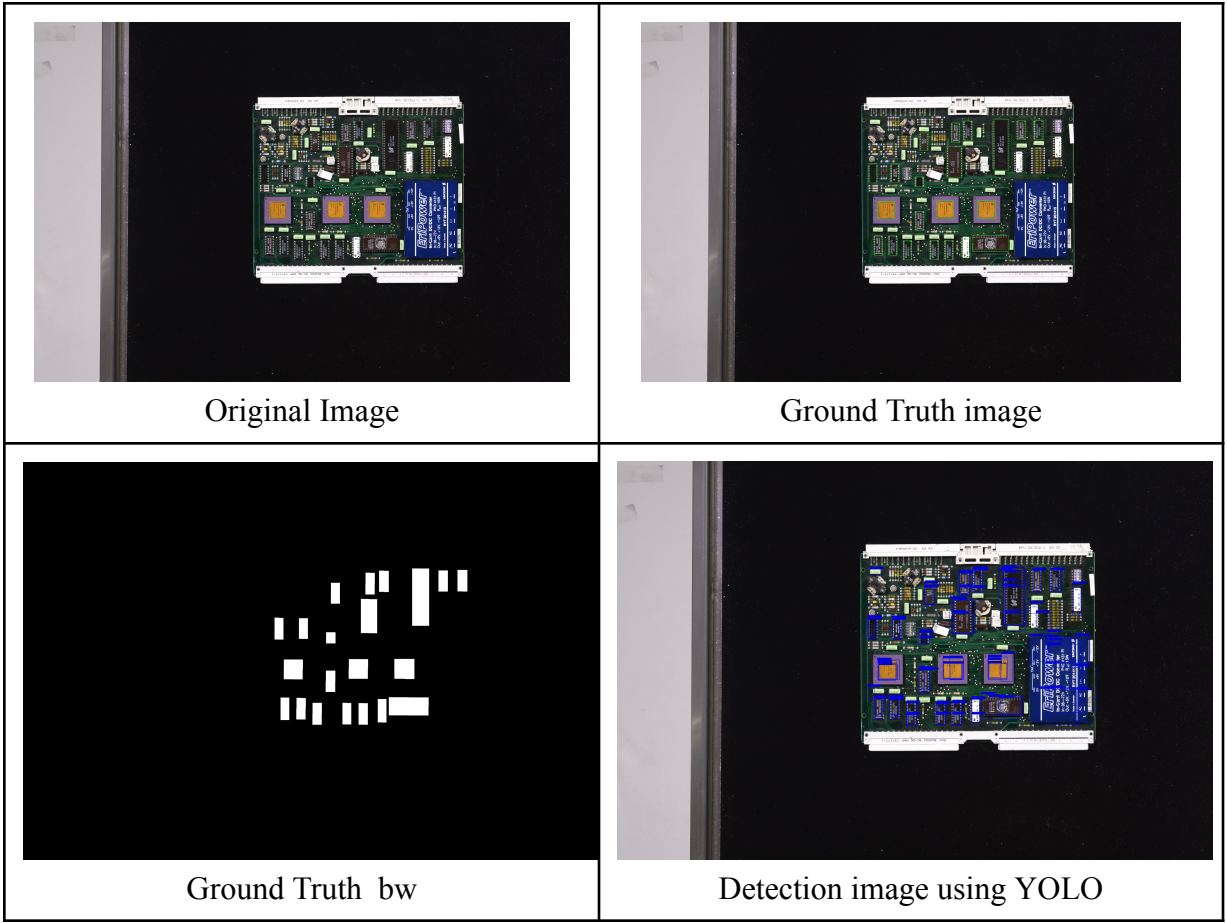


Fig 8. Sample image, annotated and detection results using YOLO from dataset[50]

FPIC Component

The FPIC Component dataset[44] originates from high-resolution PCB images captured using a Nikon D850 DSLR camera across multiple settings. The original dataset contains 93 PCB images with resolutions ranging from 2266×1832 to 8291×6929 pixels[45]. Considering the computational capability the FPIC-Component subset was focused with images cropped into patches of 768×768 pixels on individual components. The images in the dataset are also enhanced using HSI+CLAHE (Contrast Limited Adaptive Histogram Equalization).

This dataset is designed for instance segmentation, semantic segmentation, and object detection tasks relevant to the waste recycling industry. It features 6,260 images containing

29,639 labeled objects distributed across 25 classes such as Resistor (R), Capacitor (C), Integrated Circuit (U), Connector (J), Discrete Transistor (Q), Plug (P), Diode (D), Integrated Circuit (IC), and more. The dataset also provides Pixel-level instance segmentation annotations alongside training (5,008 images) and validation splits (1,252 images).

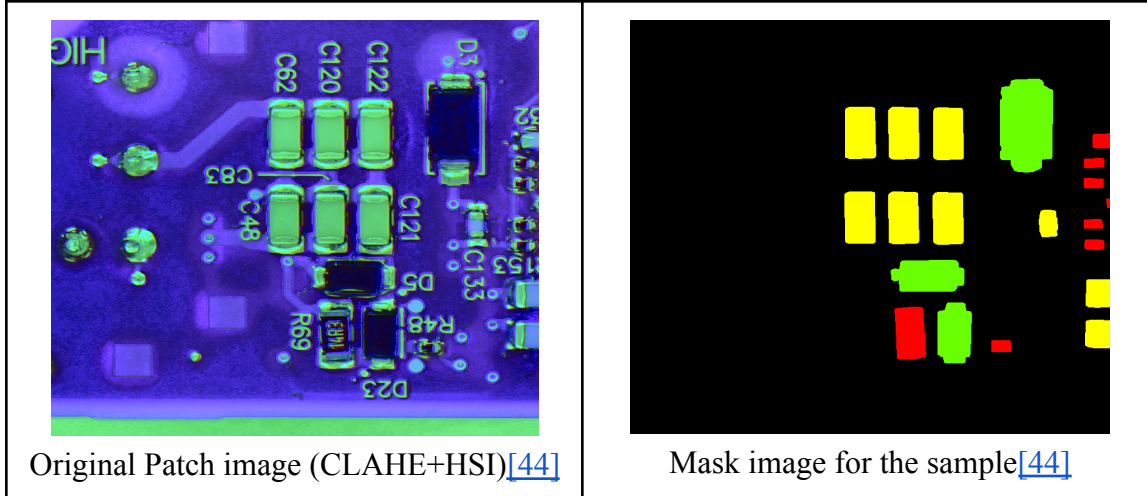


Fig 9. FPIC component dataset with 768X768 patch sample[44]

This was released by the Indian Institute of Technology in 2023 published by Makwana,

Dhruv et al.[45] on PCBSegClassNet , it supports advancements in segmentation and detection techniques for PCB analysis. However the original dataset[45] is currently restricted and not publicly available but in future they might provide a better version of it for use in research

WACV PCB dataset

The WACV PCB dataset has 47 high-resolution images with approximately 62,000 labeled component instances with 31 distinct types [51]. The large part of the components include resistors, capacitors, and connectors, resulting in a skewed distribution across classes. It also contains Pixel-level annotations that are provided for instance segmentation tasks aimed at detecting individual PCB components. The images following High-resolution imaging standards (15 megapixels or more) were given alongside dense annotations (~500 components per

PCB)[51]. The dataset aims to address challenges such as high intra-class variance and low inter-class variance while supporting automated PCB component analysis.

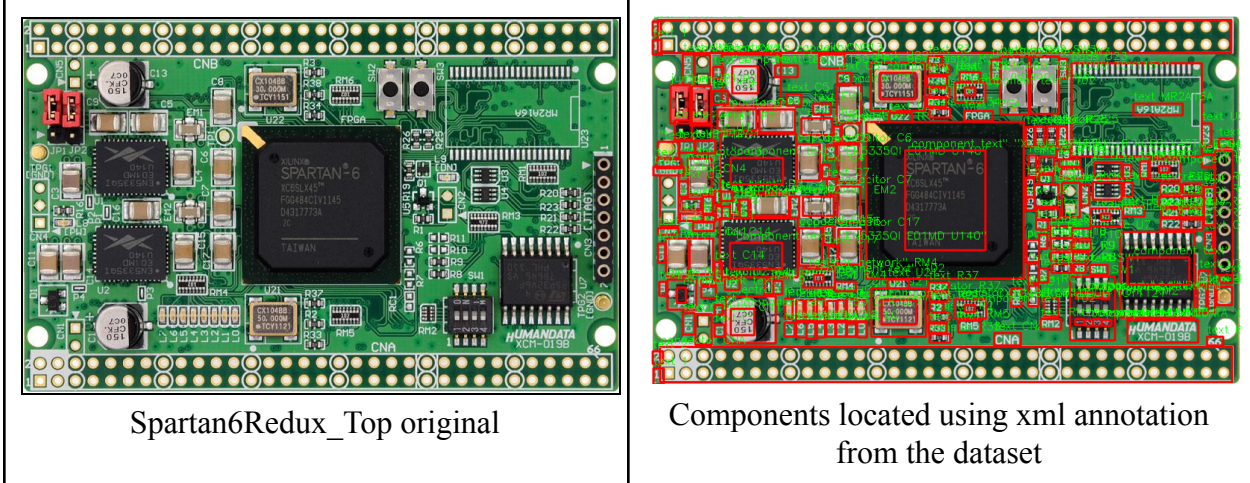


Fig 10. Sample original image and the ground truth image[51]

DeepPCB

The DeepPCB dataset consists of 1,500 image pairs that are tailored for PCB defect detection tasks including classes of six defect types: open circuit defects, short circuits, mouse bites, spurs, pinholes, and spurious copper traces. Each pair comprises a defect-free template image alongside a defective test image clipped into sub-images measuring 640×640 pixels from original scans of resolution $16k \times 16k$ captured using a linear scan CCD technology at 48 pixels per millimeter[48]. A total of 1,000 image pairs are allocated for training while the remaining 500 pairs are reserved for testing. The images are aligned using a template matching technique to minimize offset errors, also a binarization is applied to reduce illumination disturbances[48]. The images with defects are annotated with axis-aligned bounding boxes containing class IDs for localization and classification tasks.

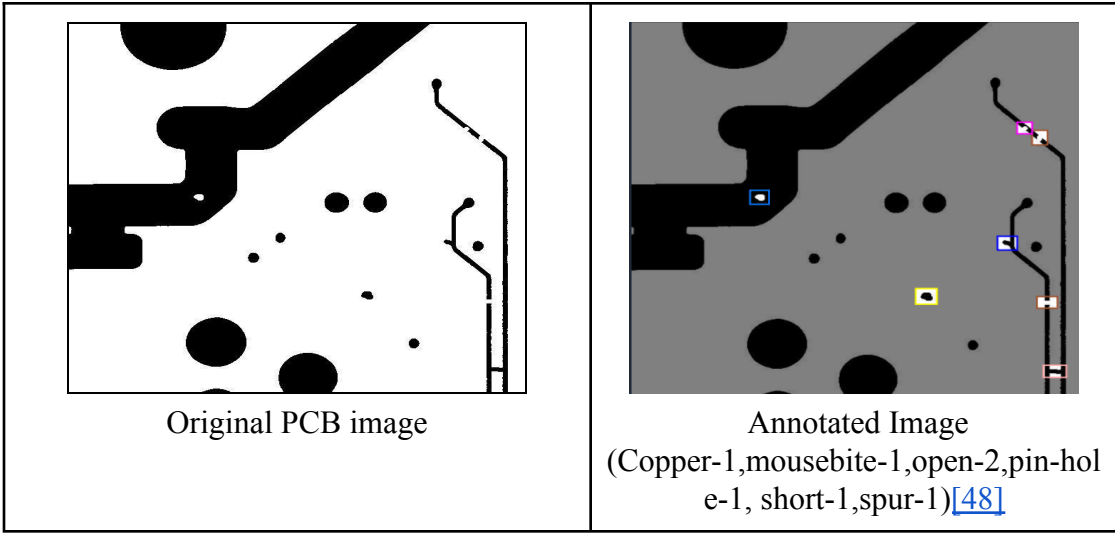


Fig 11 . Sample DeepPCB image with its annotated image [48]

Table 4 : Summary of existing datasets

Dataset	PCB Count	Data Volume	Data Type	Derivatives	Inspected Objects	Sensor Type
PCBA-defect [47]	-	1,386	RGB Images	-	6 trace defects	Digital microscope
DeepPCB [48]	-	1,500	Binary Images	-	6 trace defects	Linear scan CCD
FPIC [42]	93 (261 total images)	71,000+ s	RGB Images	Front back images; multiple settings	Text annotations and mounted components (e.g., IC, resistors, SMDs)	Nikon D850 DSLR
FPIC Component[45]	Derived from FPIC	6,260	Cropped RGB images	Instance segmentation across 25 classes	Components like C, R, U, J, L, Q, P, and others	Same as FPIC (Nikon D850 DSLR)
PCB-DSLR [50]	165	748	RGB Images	Rotation	PCB + (IC)	DSLR

PCB-Meta l [49]	123	984	RGB Images	4 rotations + front and back scans	IC, capacitors, resistors, inductors	DSLR
PCB-Visio n [19]	53	106	RGB Images + Hyperspectral	Optional derivatives provided	PCB + (IC, capacitor, connectors)	DSLR + Linescan Spectrometer
FICS-PCB [46] (Using in this study)	31	9,912	RGB Images	Illumination, scale, sensor	Capacitor, resistor, inductor, transistor, diode, IC	Digital microscope + DSLR

3.2. Introduction To Dataset

The dataset used is known as FICS-PCB [\[46\]](#), developed by the Security and Assurance (SCAN) lab at the University of Florida, is a comprehensive resource which is designed to aid research on automated Printed Circuit Board (PCB) visual inspection systems. The dataset has a total of 9,912 PCB component images [\[46\]](#) captured using DSLR cameras with large CCD sensors and digital optical microscopes at various subsets including 1x,1.5x,2x ranges [\[46\]](#). And these images are annotated with information on 77,347 components [\[46\]](#) across six classes: capacitors, resistors, transistors, diodes, inductors, and integrated circuits (ICs). The annotations are then stored in CSV formatted files, providing detailed metadata about components, their location and type.

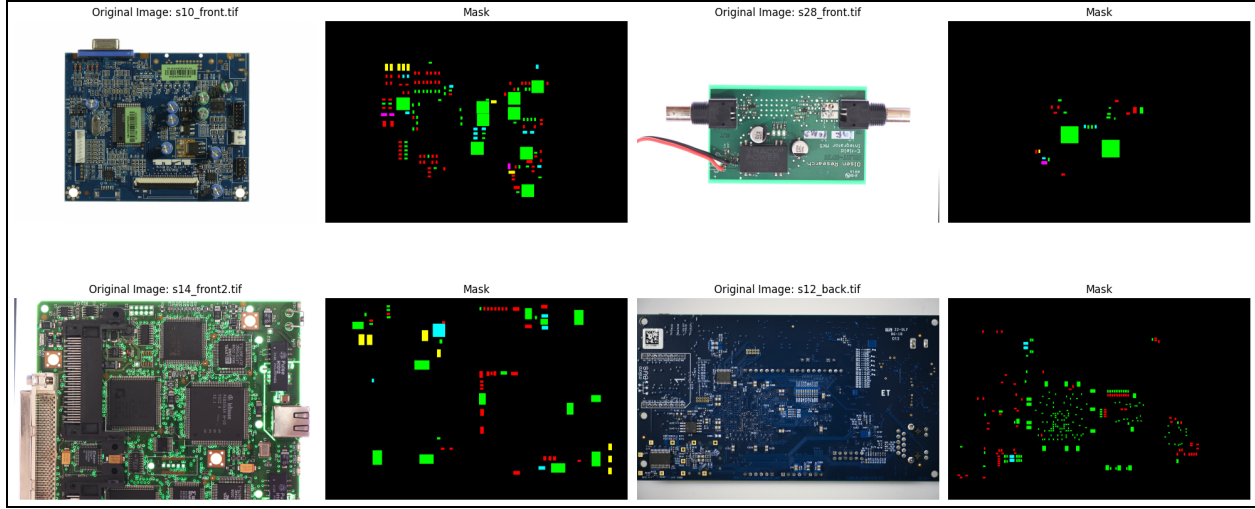


Fig 12. Sample FICS PCB images (8256x5504) with its gt-masks from the csv annotations provided excluding ICs[46]

3.2.1. Analysis of dataset components in images:

The DSLR subset from the FICS-PCB dataset contains a diverse distribution of PCB components, which is essential for robust algorithm development. Each image in this subset contains an average of 134 components, with the number of components ranging from a minimum of 13 to a maximum of 478 [46]. This variability reflects realistic scenarios encountered in e-waste recycling, where PCBs exhibit a variety of designs and configurations.

Table 5: Component Analysis in an image [46]

Modals	Subsets	Mean	Max	Min
Microscope	1x	13	101	1
	1.5x	8	90	1
	2x	6	49	1
DSLR	-	134	478	13

3.2.2. Relevance to E-Waste Recycling

The DSLR images from FICS-PCB dataset [46] will serve us as a foundation for this study , which aims to improve segmentation and detection of PCB components for effective e-waste recycling. Accurate identification of components is vital for optimizing material recovery and ensuring environmentally friendly recycling practices. By focusing on high-quality DSLR images, this study ensures precise detection, paving the way for efficient and scalable recycling solutions.

3.2. Methodologies

The primary goal of this research is to implement a robust segmentation model for accurately identifying electronic waste (E-waste) components on high-resolution PCB images. Various models and variants were selected in semantic segmentation tasks, as well as for Classification tasks. Given the complexity of the PCB images,

It is important to address the problem of featuring resolutions as high as 8256×5504 pixels[46] and multiple classes which are from ranging nearly ~478 components per image[46], a direct training was impractical due to severe GPU constraints and a substantial detail loss upon resizing. To address these challenges, a patch-based training approach was employed, involving segmenting large images into manageable patches of size 1024×1024 pixels[46], later resized to 640×640 pixels while it is optional it was recommended to fit GPU/CPU memory constraints. Special care was taken to exclude background-only patches during this preprocessing stage to optimize the training dataset for meaningful feature extraction there. Here the background represent anything other than the components of interest which is pixel value of ‘0’.

3.2.1. Models:

In this study, we experimented to evaluate the performance of various semantic segmentation and classification SOTA models including U-Net3+,U-Net, DeepLabv3+, Attention U-Net, among others. These models were chosen for their well-established capabilities in addressing semantic segmentation challenges in computer vision.

This section presents the segmentation experiments for the single channel General ground truths for RGB data images of two datasets PCB-VISION[\[19\]](#) and FICS-PCB[\[46\]](#). We tested a total of 9 most famous segmentation models with 4 including pre training. were used to benchmark the segmentation performance on both the datasets. The following methodologies section elaborates more on those models used.

Segmentation Models:

Vanilla-Unet[\[52\]\[53\]](#):

Unet is a widely used convolutional neural network (CNN) architecture for semantic segmentation tasks in computer vision especially popular in segmenting medical images datasets. The network's unique design features a symmetric U-shaped encoder-decoder structure. The Unet architecture efficiently captures multi-scale contextual information through skip connections, allowing precise segmentation of objects in images . Its effectiveness and versatility have made Unet a popular choice for various segmentation applications.

BiSeNet V2[\[77\]\[78\]](#):

A real-time semantic segmentation model that balances speed and accuracy using guided aggregation. The architecture has two branches, with wide channels and shallow layers to capture low-level details and generate high-resolution feature representation also, a Semantic

Branch, with narrow channels and deep layers to obtain high-level semantic context [77]. The Semantic Branch is lightweight due to reducing the channel capacity and a fast-downsampling strategy[77].

Deep Dual-Resolution Network (DDRNet)[78][80]:

This model is designed for road scene segmentation, it uses multiresolution processing to capture fine details while maintaining real-time efficiency. This combines low-resolution features and high-resolution features for precise boundary detection. It is a highly efficient semantic segmentation model designed for real-time scene understanding in autonomous vehicles. It addresses the challenge of balancing speed and accuracy by using two deep branches with bilateral fusion for better feature extraction. It makes segmentation more precise. DDRNet-23-slim achieves 77.4% mIoU at 102 FPS on Cityscapes[80] and 74.7% [80] mIoU at 230 FPS on CamVid, setting a new state-of-the-art trade-off between performance and efficiency.

STDC (Short-Term Dense Concatenation)[78][79]:

A lightweight efficient real-time segmentation network that improves upon BiSeNet[79] by removing redundancy and optimizing feature aggregation while also ensuring rich spatial representation for better accuracy. The aggregation module integrates spatial learning into low-level layers, enhancing feature fusion.

ResUnet[56][57]

ResUnet is a novel CNN architecture that combines the power of ResNet and Unet for semantic segmentation tasks in computer vision. The ResUnet model leverages residual connections from ResNet to facilitate efficient feature propagation during the encoder-decoder

process. This fusion enables ResUnet to capture both local and global contextual information, enhancing segmentation accuracy and robustness.

Attention Unet[\[55\]](#)[\[54\]](#)

Attention Unet is an innovative CNN architecture designed for precise semantic segmentation tasks in computer vision. The model integrates attention mechanisms within the standard Unet framework. By selectively attending to informative regions, Attention Unet achieves improved segmentation accuracy, particularly in cases where the target objects exhibit diverse appearances or complex structures. The network's attention mechanisms enable it to focus on relevant image regions, enhancing its ability to accurately delineate objects of interest, such as organs in medical imaging or objects in natural scenes.

DeepLabv3+[\[62\]](#)[\[63\]](#)

DeepLabv3+ is an advanced CNN architecture tailored for accurate semantic segmentation tasks in computer vision. The model employs an encoder-decoder structure with atrous separable convolutions . This design enables DeepLabv3+ to effectively capture multi-scale contextual information while preserving fine spatial details. In our case we tested the model using pre training with popular one that is Image and with two backbone combinations resnet34 and mit_b0 which gave good performance results

UNet3+[\[60\]](#)[\[61\]](#)

We also tested a recently popular model UNet3+ a improvised version of UNet further enriches multi-scale feature fusion by aggregating feature maps from all encoder and decoder stages at each resolution. Rather than single-level skip connections, full-scale skip pathways collect and concatenate feature maps across depths, followed by a convolutional fusion module a

little computationally expensive due to more complex structure than UNET but guarantees performance producing balanced results . This design captures both high-resolution details and global context simultaneously, yielding state-of-the-art performance on various biomedical segmentation benchmarks.

We thoroughly evaluated the results of each model's inference on the test set to comprehensively compare their performance using both the datasets in accurately segmenting our classes of interest. We also tested using few of the popular backbone architectures and pretraining techniques to compare and achieve the best possible performance using both datasets. Despite the severe class imbalance in the FICS-PCB dataset[46], some popular models still yielded promising results.

3.2.2 Data Preprocessing on the Datasets before Training:

This subsection outlines the preprocessing steps applied to the RGB data on both datasets and evaluation.

Train, validation, and test split:

As we tested using both RGB images from datasets individually where the PCB-VISION [19]dataset comprises 53 images of the 53 PCBs[19]. To facilitate effective model training, validation, and testing, we performed a split, allocating 60% of the data for training, 20% for validation, and 20% for testing. This results in 33 images used for training, 9 for validation, and 11 for testing. Then after the split we converted them to patches of 640x640 to train effectively and also considering our computational capabilities .We did not use the HSI training in our study as our focus was on segmenting RGB data[19].

And coming to the FICS-PCB[46] of the 51 images of 31 pcbs front and back we used only the front part which comprises 35 DSLR images considering the images are high resolution (8256x5504) we converted them to patches of 1024 then resized them to 640x640 to later with the train being 22 pcb images and valid and test being 7 images each the reason to experiment both dataset is to see the difference in segmentation with high quality clean images one such as FICS-PCB[46].

Data augmentation:

Data augmentation is an important technique adapted in DL that enhances models' performance by expanding the training dataset, especially with libraries like Albumentations[64], is essential for improving deep learning model performance by artificially increasing training data. This is achieved by creating data from existing samples, which addresses limited data issues and enhances model generalization. While for the pretrained models utilize a structured pipeline including resizing, flipping, rotation, brightness and contrast adjustments, normalization, and tensor conversion.

These techniques reduce overfitting problem and improve the model's ability to handle real-world scenarios, particularly in semantic segmentation where data augmentation is crucial. These transformations fall into two categories including both spatial and pixel-level transformations:

Table 6: Summary of the augmentations[64] applied on the dataset:

Data Augmentation	Details
Vertical Flip	Randomly flips images vertically with a 50% probability (p=0.5).
Horizontal Flip	Randomly flips images horizontally with a 50% probability (p=0.5).

Rotation (40°)	Rotates images randomly by up to $\pm 40^\circ$ with constant border mode ($p=0.4$).
RGB Shift	Randomly shifts RGB values of pixels (limits: ± 25 , $p=0.4$).
Color Jitter	Adjusts brightness (± 0.5), contrast (± 0.4), saturation (± 0.4), hue (± 0.2 , $p=0.4$).
Channel Shuffle	Randomly shuffles the image channels ($p=0.4$).
Transpose	Transposes image dimensions (swaps rows and columns, $p=0.4$).
Random Snow	Adds snow effects ($p=0.4$).
Shift Scale Rotate	Shifts, scales (up to 50%), and rotates with aspect ratio preserved ($p=0.4$).
OneOf (Brightness/Gamma)	Either adjusts brightness/contrast or gamma randomly (probability of each option: 40%).
OneOf (Blur/Motion Blur)	Applies either random blur or motion blur (up to 3 pixels, $p=0.4$).
OneOf (Hue/Contrast)	Applies either brightness/contrast or hue/saturation adjustments ($p=0.4$).

Applying augmentations[\[64\]](#) will ensure optimal feature extraction while maintaining stability in training pretrained models. The model increases its generalization ability to get used to the real world images, improving performance across unseen data and diverse real-world scenarios. These strategies mitigate overfitting risks, ensuring the model's efficacy in accurately segmenting components under varying lighting conditions, viewpoints, and occlusion patterns .

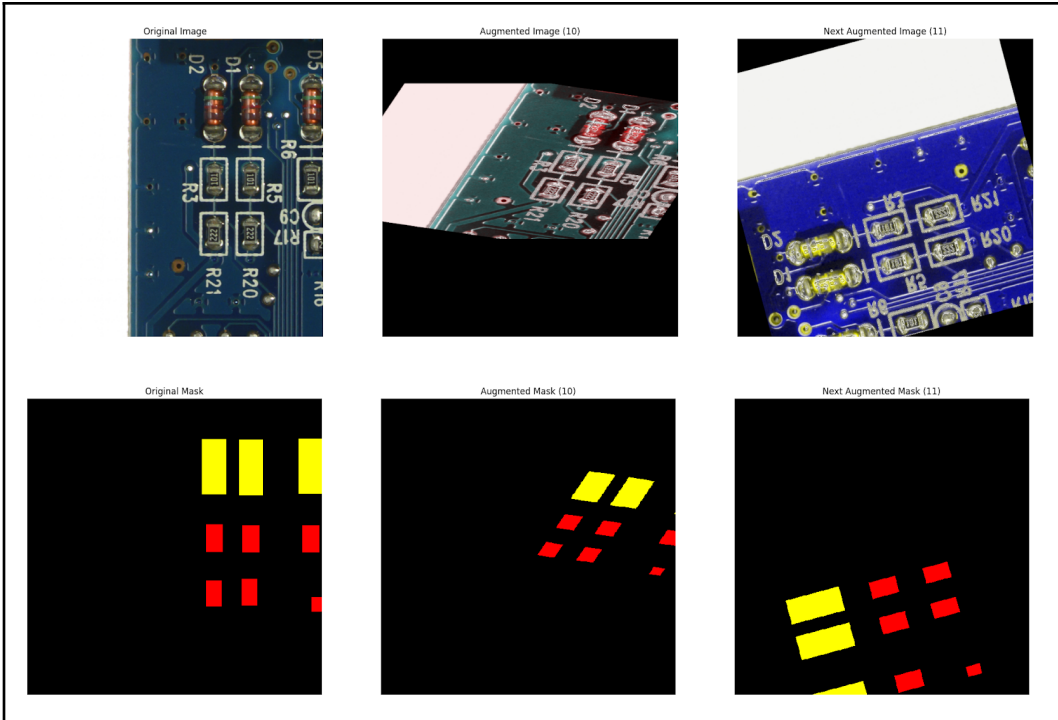


Fig 13: sample augmentation examples for the FICS-PCB dataset [46]

Class imbalance mitigation:

While our dataset comprises three classes ('IC,' 'Capacitor,' and 'Resistors') [46] another class named 'Others' is introduced for the model to classify everything that is not one of our classes of interest as 'Others'. This includes every other object that appears on the PCB surface, plus the undesired background as well. Class imbalance can impact the performance of machine learning models.

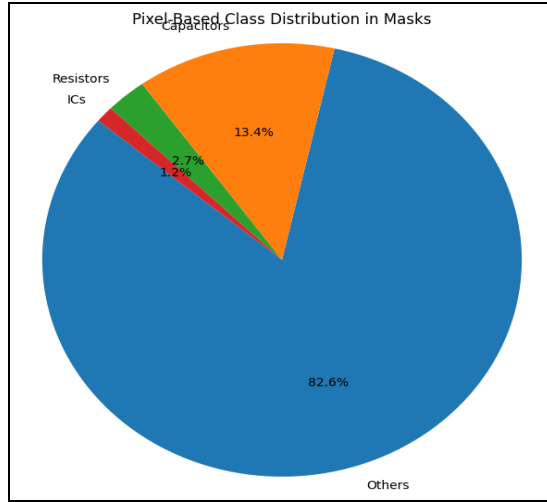


Fig 14 . Chart displaying class distribution of segmentation

To mitigate this, class weights were introduced to the loss function in order to highlight the error and updates for the classes of interest since they have fewer training samples than the 'Others' class. which worked well with PCB-VISION[19] dataset. but considering severe class imbalance in the FICS-PCB[46] dataset we did experiment with few loss functions to mitigate class imbalance and focus more on rare . minority classes.

Table 7: Class distribution based on pixel counts FICS-PCB[46]:

Class ID	Class Name	Pixel Count
0	Background	1,415,546,132
1	Resistors	88,066,407
2	Capacitors	20,238,481
3	IC	9,745,864
4	Diodes	7,362,268
5	Transistors	1,693,957
6	Inductors	2,110,539

Model Configurations:

The loss function used currently is CrossEntropyLoss with class weights however we will add more like DICE , Focal loss or even hybrid approaches to address any class imbalance problem form the training results

Table 8: Model Config for training the segmentation model:

Parameter	FICS-PCB[46](640x640)
Batch Size	8 (all models), 2 (UNet3+)
Learning Rate	0.0001
Number of Epochs	80
Class weights	[0.1,0.8,0.85,0.9]
Loss Functions	Hybrid: Weighted CrossEntropy(WCCE)+ DICE loss
Optimizer	Adam
Training Samples (images,masks pair)	22 pcbs-FICS-PCB[46] 33pcbs for PCB-VISION[19]
Validation Samples (images,masks pair)	7 pcbs -FICSPCB[46], 9 pcbs, PCB-VISION[19]

Loss functions Used:

Weighted Categorical Cross-Entropy (WCCE)

To counter severe class imbalance problems where rare components such as inductors, transistors, and diodes co-exist with large components like ICs. We assigned a per-class weight W_c in cross-entropy[65]. Given N pixels, C classes, one-hot labels $y_{n,c} \in \{0,1\}$, and predicted probabilities $p_{i,c}$, the loss is:

$$l_n = - \sum_{c=1}^C w_c \log \frac{\exp(x_{n,c})}{\sum_{i=1}^C \exp(x_{n,i})} y_{n,c}$$

Multiclass Dice Loss.

Dice loss [66] measures overlap between prediction and ground truth, directly optimizing region agreement. For each class.

$$\mathcal{L}_{\text{Dice}} = 1 - \frac{1}{C} \sum_{c=1}^C \frac{2 p_c^\top y_c + \varepsilon}{\|p_c\|_1 + \|y_c\|_1 + \varepsilon}.$$

Hybrid Loss: Weighted CCE [65]+ Dice[66]:

To balance pixel-wise accuracy and region overlap mitigating WCCE's [65] overfitting on FICS-PCB dataset we added a DICE [66] loss to the WCCE [65] to undergo a balanced training with no overfitting.

$$\begin{aligned} \mathcal{L}_{\text{hybrid}} &= \frac{1}{2} \mathcal{L}_{\text{WCCE}} + \frac{1}{2} \mathcal{L}_{\text{Dice}}, \\ \mathcal{L}_{\text{WCCE}} &= -\frac{1}{N} \sum_{n=1}^N \sum_{c=1}^C w_c y_{n,c} \log \left(\frac{\exp(x_{n,c})}{\sum_{k=1}^C \exp(x_{n,k})} \right), \\ \mathcal{L}_{\text{Dice}} &= 1 - \frac{1}{C} \sum_{c=1}^C \frac{2 \sum_{n=1}^N p_{n,c} y_{n,c} + \varepsilon}{\sum_{n=1}^N p_{n,c} + \sum_{n=1}^N y_{n,c} + \varepsilon}, \end{aligned}$$

with $\alpha=0.5$ [\[66\]](#). This hybrid loss leverages WCCE's[\[65\]](#) class weighting and Dice's[\[66\]](#) region-based penalization, yielding more stable training and improved focus on under-represented PCB components.

3.4. Evaluation Metrics

For comparison and performance evaluation we used several key metrics which were selected to comprehensively evaluate segmentation .We used many metrics for evaluation but the only metric that evaluates segmentation is IOU and DICE scores and remaining are used for additional details.

Pixel Accuracy[\[67\]](#): This measures the fraction of correctly classified pixels, giving a global sense of overall segmentation quality.

$$\text{Acc} = \frac{\sum_c TP_c}{\sum_{i,j} CM_{i,j}}$$

Intersection over Union (IoU)[\[67\]](#)[\[76\]](#): the overlap ratio between predicted and ground-truth regions, directly assessing segmentation accuracy on a per-class basis.

$$\text{IoU}_c = \frac{TP_c}{TP_c + FP_c + FN_c}$$

Dice Score[\[67\]](#): twice the overlap over the total region size, emphasizing correct region alignment and commonly used for highly imbalanced segmentation tasks.

$$\text{Dice}_c = \frac{2TP_c}{2TP_c + FP_c + FN_c}$$

For Classification: For classification we used many metrics such as f1-score, accuracy , recall , precision, MCC:

Precision : Measures the proportion of predicted positives that are true positives:

$$\text{Precision} = \frac{TP}{TP + FP}$$

Recall : Measures the proportion of actual positives that are correctly predicted:

$$\text{Recall} = \frac{TP}{TP + FN}$$

F1-Score: The harmonic mean of precision and recall, balancing the two:

$$F1 = 2 \times \frac{\text{Precision} \times \text{Recall}}{\text{Precision} + \text{Recall}}$$

Accuracy : The fraction of all correct predictions (both positive and negative):

$$\text{Accuracy} = \frac{TP + TN}{TP + TN + FP + FN}$$

Matthews Correlation Coefficient (MCC) : It is balanced measure taking into account TP, TN, FP, and FN:

$$MCC = \frac{TP \times TN - FP \times FN}{\sqrt{(TP + FP)(TP + FN)(TN + FP)(TN + FN)}}$$

3.5. Proposed Approach

Successfully implemented patch-based training on high-resolution PCB images (8256×5504)[\[46\]](#), preserving critical component details while fitting GPU memory constraints using various SOTA segmentation models and also experimented with many popular models for classification .

- Designed and executed an extensive data augmentation pipeline (geometric transforms, color jitter, noise) that improved model robustness to diverse PCB imaging conditions.
- Addressed severe class imbalance through targeted class-weighted CrossEntropy loss,DICE loss and Hybrid loss, enabling the model to learn effectively across seven component classes.
- Demonstrated strong segmentation performance and classification performance using various models.

RESULTS AND ANALYSIS

4.1 Model Performance and Results

Sample images from Dataset:

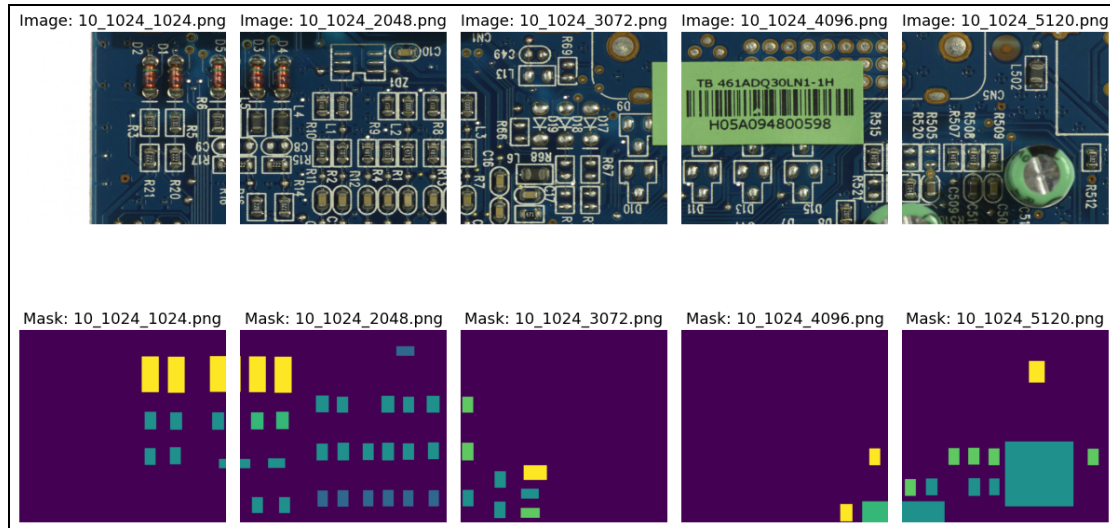


Fig 15: Sample extracted patches (1024×1024 crops resized to 640×640)[46]

Segmentation Results for PCB-VISION [19]dataset Weighted-CCE loss function[65]:

Test Images	Original Image 1	Original Image 2	Original Image 3	Original Image 4	Original Image 5
Ground Truth	Ground Truth 1	Ground Truth 2	Ground Truth 3	Ground Truth 4	Ground Truth 5

Unet [52][53](2015)	Predicted Mask 1	Predicted Mask 2	Predicted Mask 3	Predicted Mask 4	Predicted Mask 5
Attention-Unet [55][54](2018)	Predicted Mask 1	Predicted Mask 2	Predicted Mask 3	Predicted Mask 4	Predicted Mask 5
ResUnet [56][57](2017)	Predicted Mask 1	Predicted Mask 2	Predicted Mask 3	Predicted Mask 4	Predicted Mask 5
Unet-Mobil eNtv2 [58] [59](2018)	Predicted Mask 1	Predicted Mask 2	Predicted Mask 3	Predicted Mask 4	Predicted Mask 5
Unet++ (Nested Unet)[74](2018)	Predicted Mask 1	Predicted Mask 2	Predicted Mask 3	Predicted Mask 4	Predicted Mask 5
Vgg16-Une t(pretrained)[75](2015)	Predicted Mask 1	Predicted Mask 2	Predicted Mask 3	Predicted Mask 4	Predicted Mask 5

Fig 16.. Segmentation Results for PCB-VISION with WCCE loss function [19]

Segmentation Results on FICS-PCB Dataset[46] with only Weighted-CCE loss function[65]

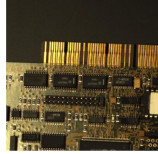
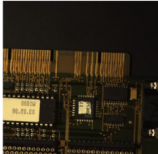
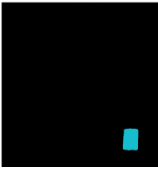
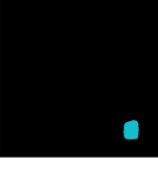
Sample Test images	Original Image 1	Original Image 2	Original Image 3	Original Image 4	Original Image 5
Ground Truth	Ground Truth 1	Ground Truth 2	Ground Truth 3	Ground Truth 4	Ground Truth 5
ResUnet [56][57] (2017)	Predicted Mask 1	Predicted Mask 2	Predicted Mask 3	Predicted Mask 4	Predicted Mask 5
Attention- Unet [55][54] (2018)	Predicted Mask 1	Predicted Mask 2	Predicted Mask 3	Predicted Mask 4	Predicted Mask 5
Unet-Mobil eNtv2 backbone [58] [59](2018)	Predicted Mask 1	Predicted Mask 2	Predicted Mask 3	Predicted Mask 4	Predicted Mask 5

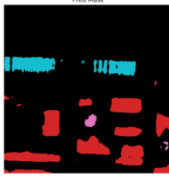
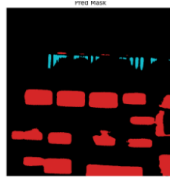
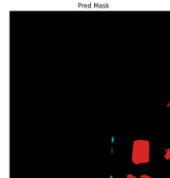
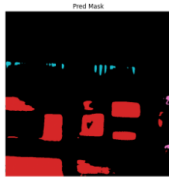
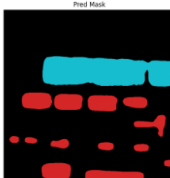
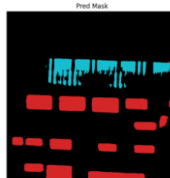
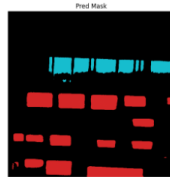
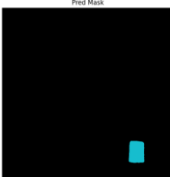
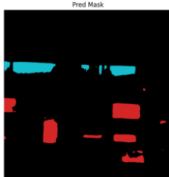
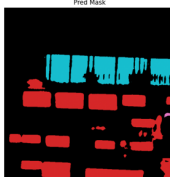
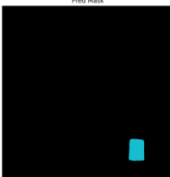
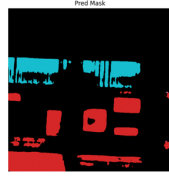
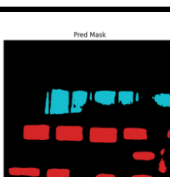
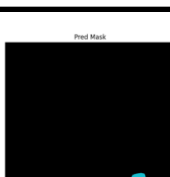
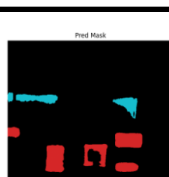
Fig 17. Segmentation Results for FICS-PCB with WCCE loss function [46]

Conclusion: We can observe from above that there is a severe class imbalance problem and the loss function is not effective in segmenting the minority classes so we try with a Hybrid

approach adding DICE loss to it and some of the model results are below using the hybrid loss function.

Segmentation Results for PCB-VISION[\[19\]](#) dataset(with better results)[\[65\]](#)[\[66\]](#):

Original images			
Ground truth images			
Attention-Une t [55] [54] (2018)			
Bisenetv2 [77] [78] (2020)			
Drdnet [78] [80] [1] (2021)			
ResUnet [56] [57] (2017)			

Unet-MobileN tv2 backbone [58] [59] (2018)			
Unet-Vgg16 [7] [5] (2015)			
STDC [78] [79] (2021)			
UNET [52] [53] [1] (2015)			
UNET++ [74] (2018)			
UNet3+ [60] [61] without cgm and deep supervision (2020)			
DeepLabV3+ [62] [63] with Backbone: mit-b0, imagenet (2021)			

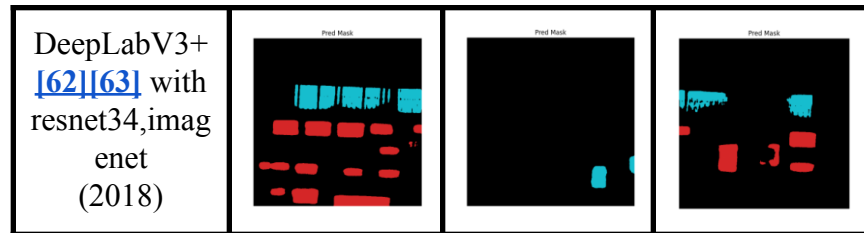
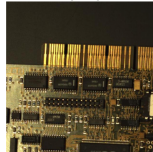
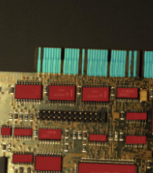
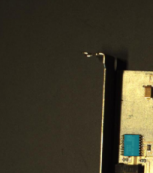
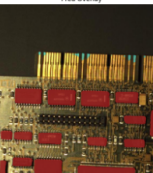
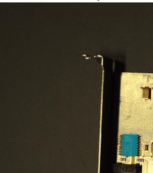
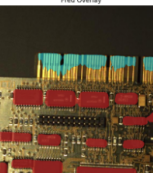
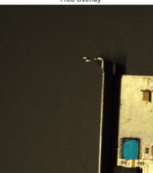
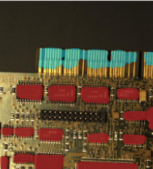
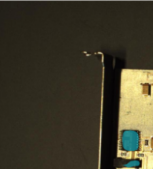
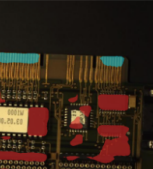
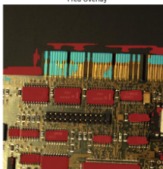
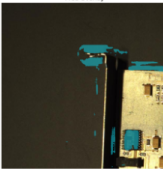
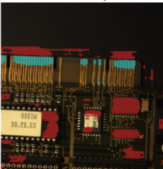
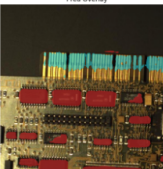
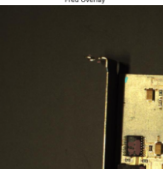
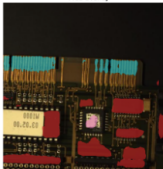
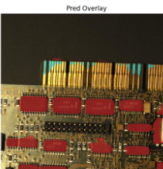
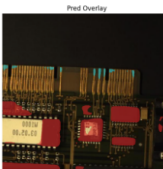
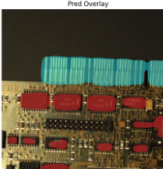
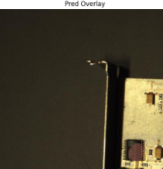
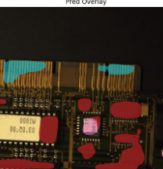
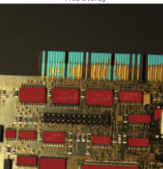
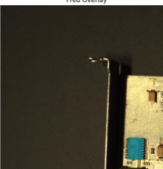
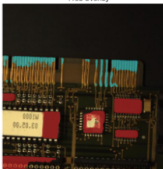
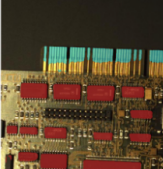
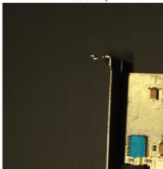
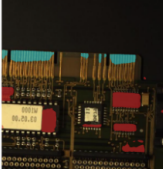
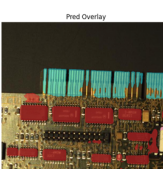
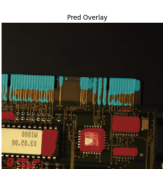


Fig 18: Predicted Masks using Hybrid loss function

Segmentation Results for PCB-VISION[\[19\]](#) dataset(with better results)[\[65\]](#)[\[66\]](#):

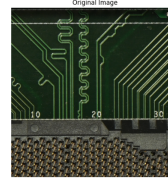
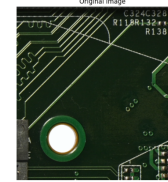
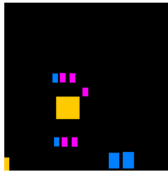
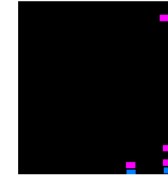
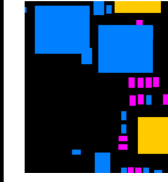
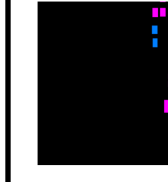
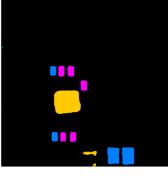
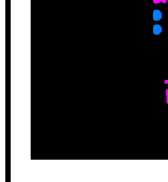
Original images	 Original Image	 Original Image	 Original Image
Ground truth images	 GT Overlay	 GT Overlay	 GT Overlay
Attention-Une t [55] [54] (2018)	 Pred Overlay	 Pred Overlay	 Pred Overlay
Bisenetv2 [77] [78] (2020)	 Pred Overlay	 Pred Overlay	 Pred Overlay
Drdnet [78] [80] (2021)	 Pred Overlay	 Pred Overlay	 Pred Overlay

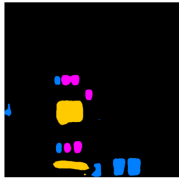
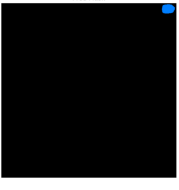
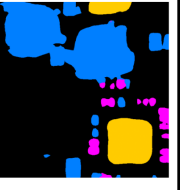
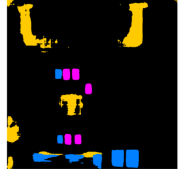
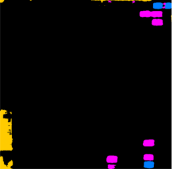
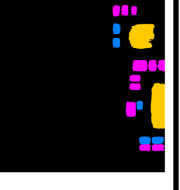
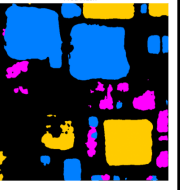
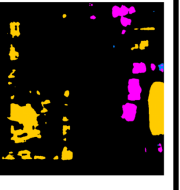
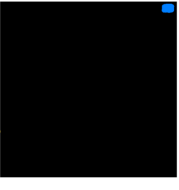
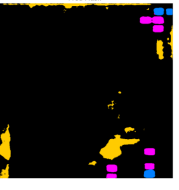
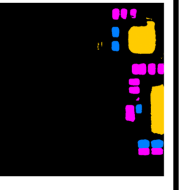
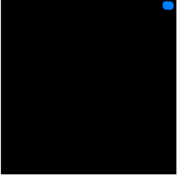
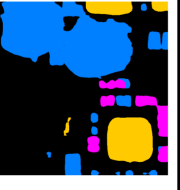
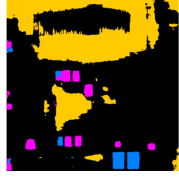
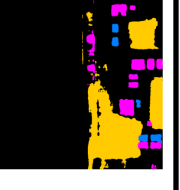
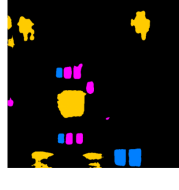
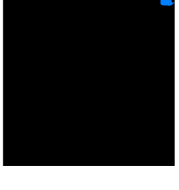
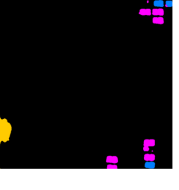
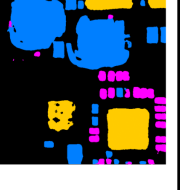
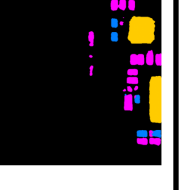
<p>ResUnet [56][57] (2017)</p>			
<p>Unet-MobileN tv2 backbone [58] [59](2018)</p>			
<p>Unet-Vgg16[7] [5] (2015)</p>			
<p>STDC[78] [79] (2021)</p>			
<p>UNET[52][53] [1] (2015)</p>			
<p>UNET++ [74] (2018)</p>			
<p>UNet3+ [60][61] without cgm and deep supervision</p>			

(2020)			
DeepLabV3+[62][63] with Backbone: mit-b0, imagenet (2021)	Pred Overlay	Pred Overlay	Pred Overlay
DeepLabV3+[62][63] with resnet34,imagenet (2018)	Pred Overlay	Pred Overlay	Pred Overlay

Fig 19. Predicted Masks overlays

Segmentation Results for FICS-PCB[[46](#)] dataset(with better results)[[65](#)][[66](#)]:

Original images					
Ground truth images					
Attention-Unet [55][54] (2018)					
Bisenetv2 [77] [78] (2020)					

Drnet[78][80] (2021)					
ResUnet [56][57] (2017)					
Unet-Mobile Ntv2 backbone [58] [59](2018)					
Unet-Vgg16[75] (2015)					
STDC[78] [79] (2021)					
UNET[52][53] (2015)					
UNET++ [74] (2018)					

UNet3+ [60] [61] without cgm and deep supervision (2020)	GT Mask	Pred Mask	Pred Mask	Pred Mask	Pred Mask
DeepLabV3+ [62] [63] with Backbone: mit-b0, imagenet (2021)	Pred Mask				
DeepLabV3+ [62] [63] with resnet34,ima genet (2018)	Pred Mask				

Fig 20. Predicted Masks using FICS-PCB[\[46\]](#):

Segmentation Results for FICS-PCB[\[46\]](#) dataset(with better results)[\[65\]](#)[\[66\]](#):

Original images	Original Image	Original Image	Original Image	Original Image
Ground truth images	GT Overlay	GT Overlay	GT Overlay	GT Overlay
Attention-Un et [55] [54] (2018)	Pred Overlay	Pred Overlay	Pred Overlay	Pred Overlay

Bisenetv2 [77] [78] (2020)					
Drdnet[78][80] (2021)					
ResUnet [56][57] (2017)					
Unet-Mobile Ntv2 backbone [58] [59](2018)					
Unet-Vgg16[75] (2015)					
STDC[78] [79] (2021)					
UNET[52][53] (2015)					

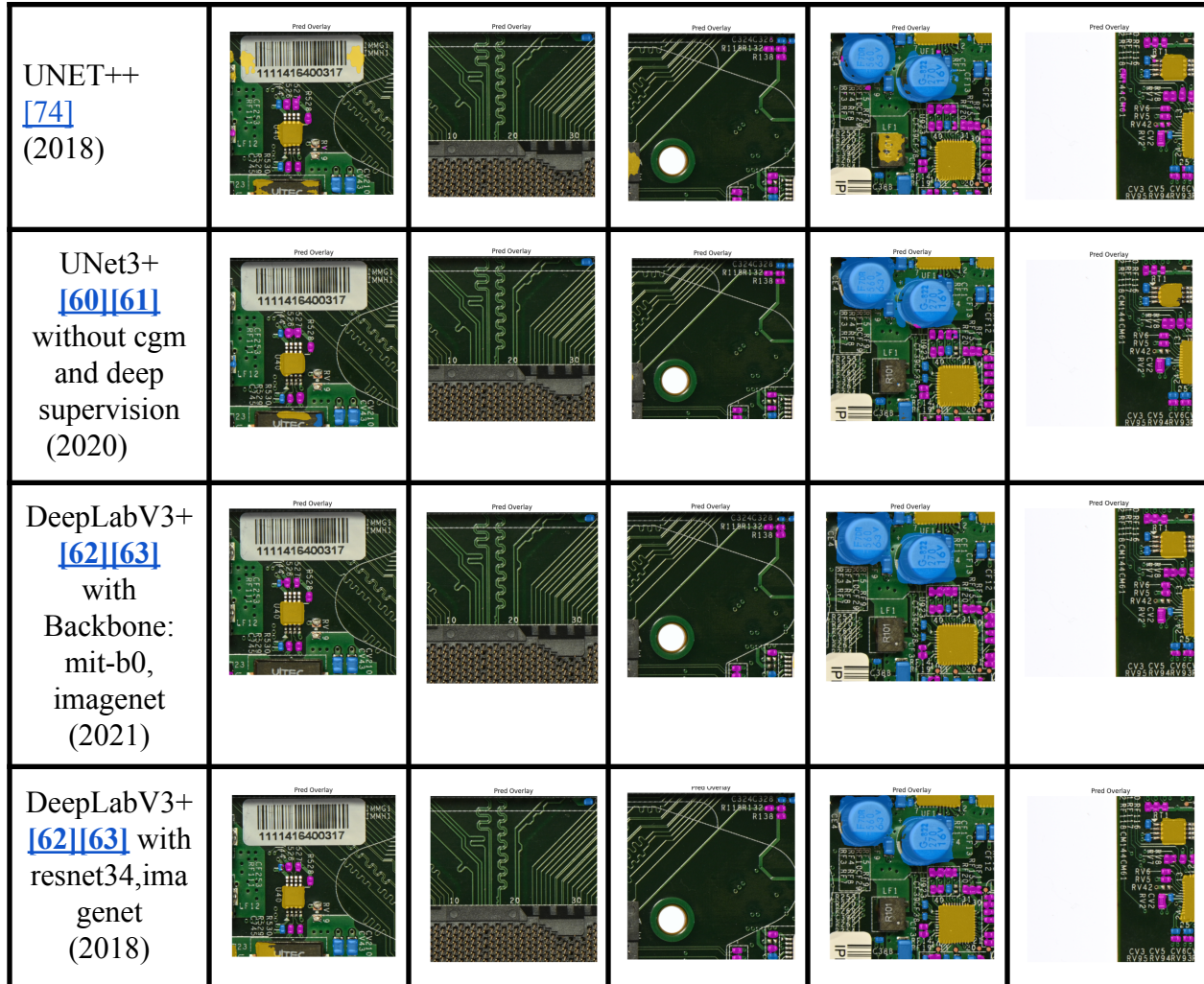


Fig 21. Predicted Masks overlays

4.2 Comparative Analysis

For performance comparison we used various models for segmenting both PCB Vision dataset[19] and FICS-PCB[46] dataset also Patch Training for better and more detailed segmentation of components. The below are the results obtained from the models used in training both our datasets individually for comparing the performance also addressing class Imbalance

Table 9: Segmentation results using Pre Training on PCB-VISION dataset[19]:

Model	Pretrained	DICE (mean)	IOU (mean)	Pixel Accuracy	Parameter Count (M)	Model Size
-------	------------	----------------	---------------	-------------------	------------------------	---------------

UNet-MobileNet V2 [58] [59] (2018)	MobileNetV2	68.13%	54.90%	91.03%	~15	57
VGG16-UNet [75] (2015)	VGG16 Encoder	81.14%	69.53%	94.95%	~41	159
DeepLabV3+ with resnet34 [62][63] (2018)	ImageNet	86.87%	77.55%	97.96%	~4.1	16.65
DeepLabV3+ with mit_bo [62][63] (2021)	ImageNet	87.05%	78.90%	98.19%	~4.1	16.65

Table 10: Segmentation results without using Pre Training on PCB-VISION dataset [19]:

Model	Pretrained	DICE (mean)	IOU (mean)	Pixel Accuracy	Parameter Count (M)	Model Size
ResUNet [56][57] (2017)	No	69.76%	57.16%	94.25%	~13	49
UNet [52][53] (2015)	No	80.38%	69.61%	97.79%	~31	118
Drdnet [78][80] (2021)	No	75.86	63.65	96.52	~5.5	21.14
Bisenetv2 [77] [78] (2020)	No	71.91	60.49	96.69	~2.2	8.66
STDC [78] [79] (2021)	No	70.03	56.46	94.00	~7.7	29.70
Nested UNet (UNet++) [74] (2018)	No	77.83%	66.65%	97.66%	~9	34
AttU-Net [55][54] (2018)	No	68.66%	60.57%	97.75%	~34	133
UNet3+ [60][61] (2020)	No	83.58%	74.05%	97.80%	~26.9	102.86

Table 11: Segmentation results using Pre Training on FICS-PCB dataset [46]

Model	Pretrained	DICE (mean)	IOU (mean)	Pixel Accuracy	Parameter Count (M)	Model Size
VGG16-UNet [75] (2015)	VGG16 Encoder	81.19%	69.15%	91.37%	~41	159
UNet-MobileNet V2 [58] [59] (2018)	MobileNetV2	73.64%	59.78%	88.35%	~15	57
DeepLabV3+ with resnet34 [62] [63] (2018)	ImageNet	91.20%	84.33%	97.54%	~4.1	16.65
DeepLabV3+ with mit_bo [62] [63] (2021)	ImageNet	89.73%	81.86%	96.72%	~4.1	16.65

Table 12: Segmentation results without using Pre Training on FICS-PCB dataset[\[46\]](#)

Model	Pretrain ed	DICE (mean)	IOU (mean)	Pixel Accuracy	Parameter Count (M)	Model Size
ResUNet [56] [57] (2017)	No	74.29%	60.49%	86.42%	~13	49
UNet [52] [53] (2015)	No	76.22%	62.65%	87.10%	~31	118
Nested UNet (UNet++) [74] (2018)	No	82.11%	70.46%	92.16%	~9	34
Drdnet [78] [80] (2021)	No	78.32	65.72	91.79	~5.5	21.14
Bisenetv2 [77] [78] (2020)	No	79.33	67.16	92.84%	~2.2	8.66
STDC [78] [79] (2021)	No	80.40	68.61	92.96%	~7.7	29.70
UNet3plus [60] [61] [1] (2020)	No	73.88%	60.39%	84.49%	~26.9	102.86
Attention-Unet	No	80.17%	68.01%	92.68%	~34	133

4.3 Result Analysis:

4.3.1. Impact of Pretraining

From both PCB-VISION[19] and FICS-PCB[46] datasets, we can observe that initializing with pretrained encoders elevated segmentation quality the two datasets employed which are RGB images have severe class imbalance problem especially in FICS-PCB[46] considering more samples for frequent and very few for rare classes we also introduced new class that is background (includes other components). So training from the scratch to get highly accurate segmentation requires focus on each class based on its distribution we have tried different loss functions and also different weights strategies however due to its severity we still managed to optimize better results in segmentation. With more work on addressing class imbalance problems we can get more optimised and high performance on any dataset . As our focus is solely on RGB images and e-waste recycling the two dataset employed were tested and evaluated across multiple models with various techniques.

On PCB-VISION[19], the two DeepLabV3+ variants led the pretrained group—MiT-B0 attained the highest DICE score (87.05 %) and pixel accuracy (98.19 %), also closely followed by ResNet34 (86.87 % DICE, 97.96 %)[62][63].

On FICS-PCB[46], ResNet34 edged out MiT-B0 with a remarkable 91.20 % DICE and 84.33 % IOU. These pretrained models required only ~4 M parameters and <17 MB of storage, demonstrating that compact backbones can deliver top-tier accuracy when fine-tuned.

4.3.2. Training from Scratch

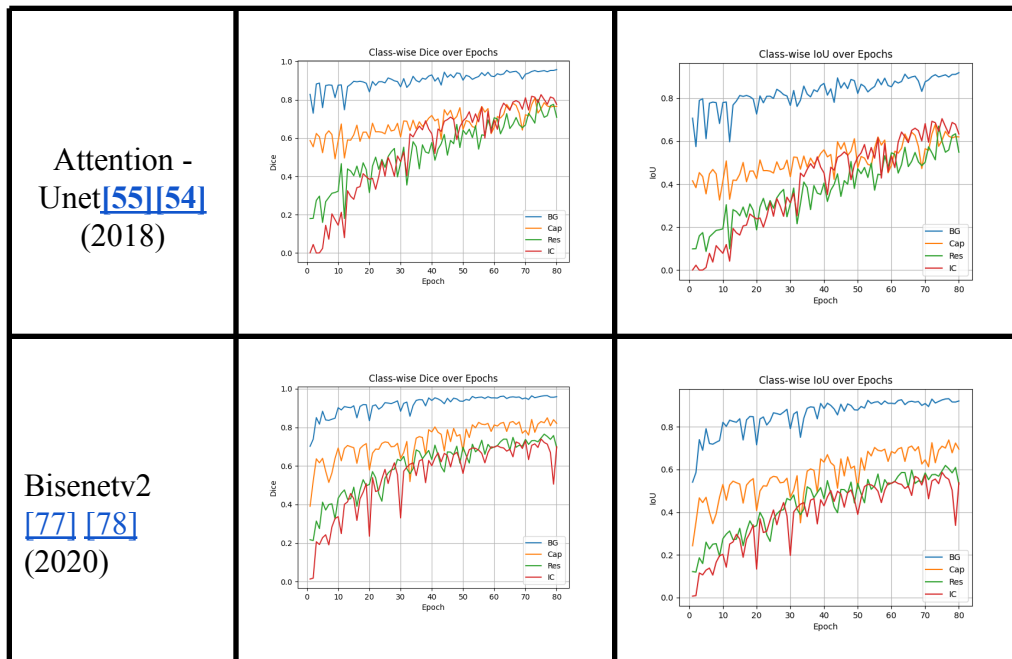
When trained without using a pre-trained approach, networks such as nested and multi-scale skip-connection architectures got better results. On PCB-VISION[19], UNet3plus[60][61] topped the non-pre trained networks with 83.58 % DICE and 74.05 % IOU, which outperformed heavier models like VGG16-UNet[75] despite using fewer parameters. Same goes for FICS-PCB[46], Nested UNet (UNet++)[74] achieved the highest DICE (82.11 %) and IOU (70.46 %). These results underscore the strength of dense skip connections in capturing PCB components edges without relying on external pre-training; however it still needs improvement in segmentation in precision with edges as it still struggles with overlapping and some mis-classifications which can be overcome with more training and better loss functions and weights distribution strategies.

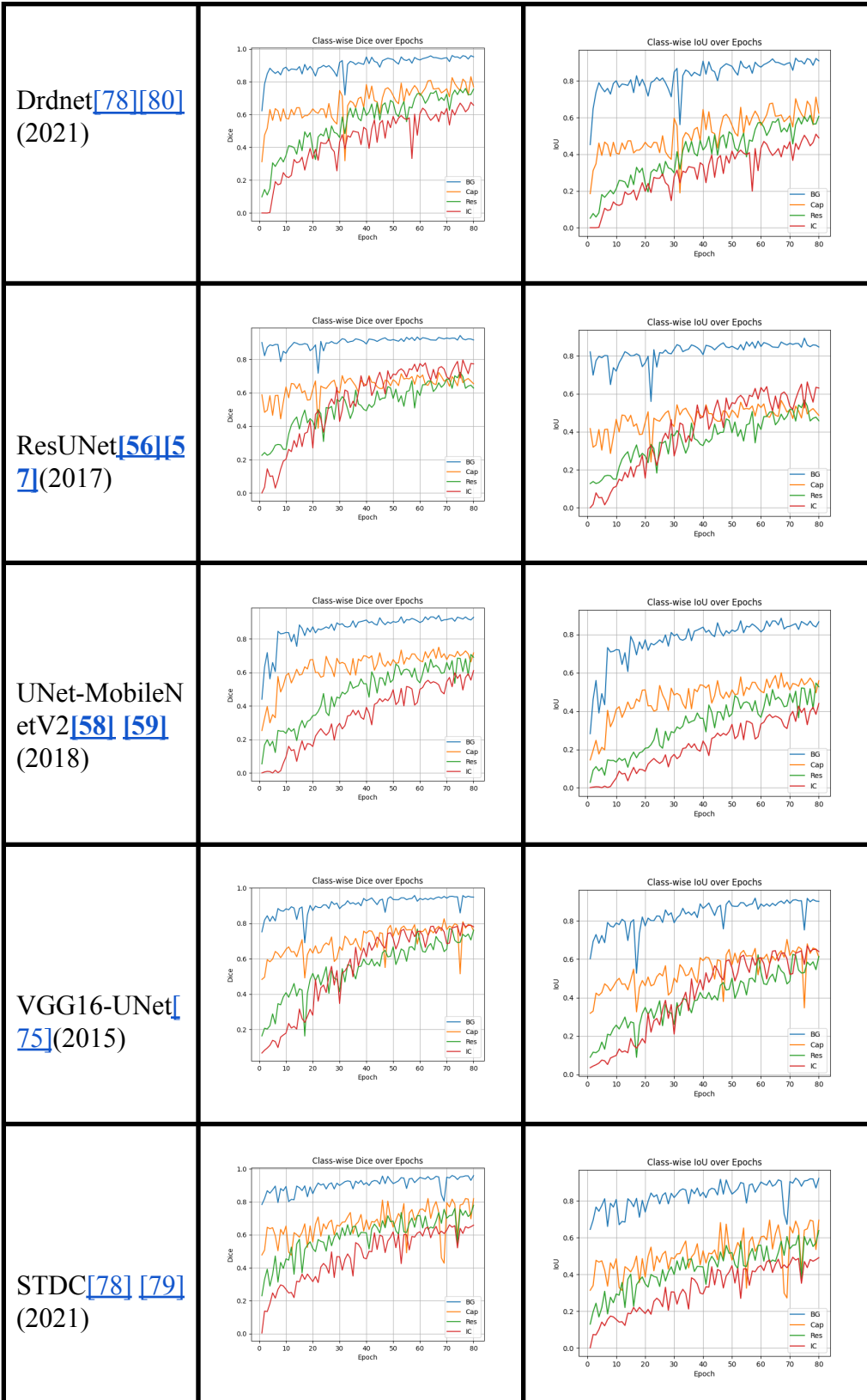
4.3.3. Summary

Pretraining yields the largest gains for compact, context-rich backbones—DeepLabV3+[62][63] variants dominate both datasets with minimal overhead. When pretraining is unavailable, architectures with nested skip connections (UNet3plus[60][61], Nested-UNet[74]) best recover segmentation performance, albeit at higher storage and parameter cost.

- **Best overall performance:** DeepLabV3+ (ResNet34/MiT-B0)[\[62\]](#)[\[63\]](#) balances sub-4 M parameters and <17 MB[\[62\]](#)[\[63\]](#) with top DICE (>86 %) and pixel accuracy (>97 %) when pretrained.
- **Best without pre training:** UNet3+ [\[60\]](#)[\[61\]](#) and Nested UNet[\[74\]](#) deliver strong DICE (~83 %) and IOU (~74 %) but incur larger model sizes (34–103 MB).
- **Lightweight models:** (MobileNetV2[\[59\]](#), BiSeNetV2[\[77\]](#) [\[78\]](#), STDC[\[78\]](#)[\[79\]](#)) lag by 5–20 % in DICE, indicating limited representation capacity unless pretrained.

Below are DICE and IOU graphs for comparison on performance across each class for different models.





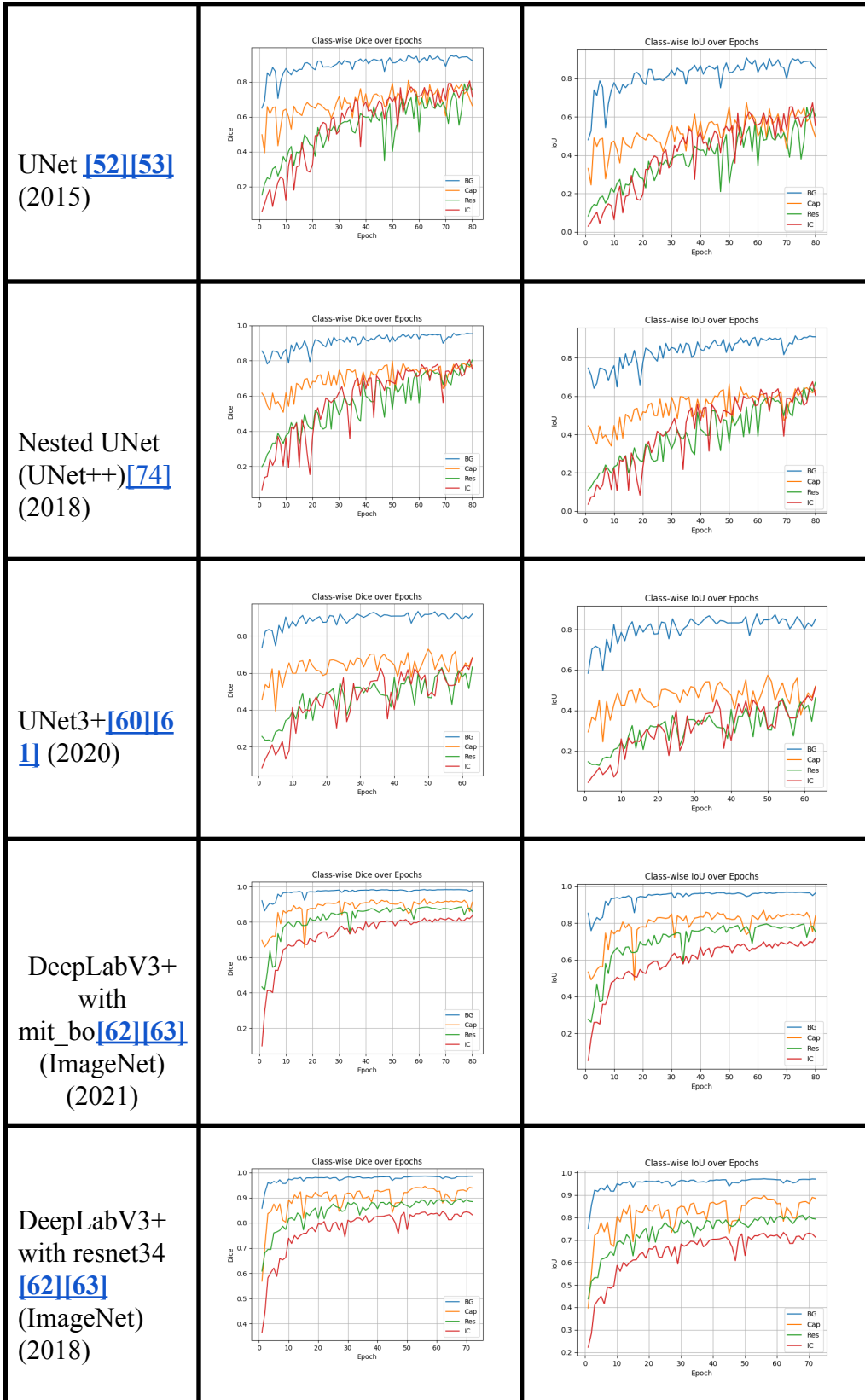


Fig 22. Class-wise DICE and IOU metrics graphs for FICS-PCB[\[46\]](#) images

4.4 Classification Models:

Dataset: We are using our FICS-PCB dataset[46] for performing classification of components of our interest including common and rare components such as Resistors, Capacitors, ICs, Transistors, Inductors, Diodes and the dataset has lot of variability in components making it a best suitable dataset for PCB-component classification.

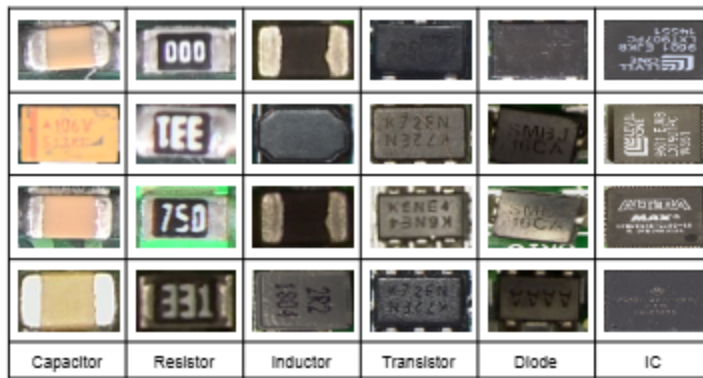


Fig 23. labeled FICS-PCB[46] components from the dataset.[68]

From the given composition below we only used 762 samples for training of each of 6 classes and rest for testing the results were from 200 test samples each class.

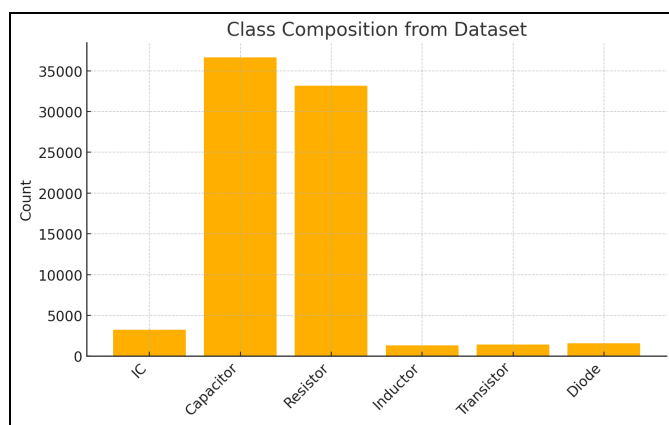


Fig 24. FPIC-PCB[46] class composition[68]

4.4.1. Methodologies:

A total of 5 most recent popular models were used in classifying 6 components of interest from the FICS-PCB[46] dataset.

PCBClassNet[\[44\]](#)

A lightweight convolutional network for PCB component classification extracted from PCBSegClassNet by (Makwana, D, 2022)[\[44\]](#) is a two-branch network for achieving high segmentation and classification which uses texture enhancement (TEM) module a Global average pooling in their network[\[44\]](#).

DInPNet[\[68\]](#)

A custom architecture named DInPNet by (Makwana, D, 2023)[\[68\]](#) based on Involution and DInP block for PCB components classification are the first to use and implement PCB component classification on FPIC-PCB Dataset .

EfficientNetV2[\[70\]](#)[\[71\]](#)

An efficient architecture that jointly scales depth, width and resolution using a mix of Fused-MBConv and MBConv blocks, enabling faster training and better parameter efficiency. (Tan & Le, 2021)[\[71\]](#)

MobileNetV3[\[69\]](#)

Designed via platform-aware neural architecture search, it features inverted residual bottlenecks with squeeze-and-excitation, hard-swish activations, and lightweight attention modules for a favorable latency–accuracy trade-off. (Howard et al., 2019)[\[69\]](#)

ConvNeXt-Tiny[\[72\]](#)[\[73\]](#)

A modern ConvNet that rethinks ResNet design by adopting Vision-Transformer-inspired elements—large kernels, LayerNorm, inverted bottlenecks—while remaining purely convolutional. (Liu et al., 2022)[\[73\]](#)

4.5 Classification Performance results on FICS-PCB Dataset[\[46\]](#):

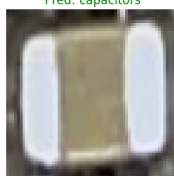
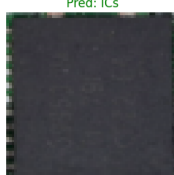
Table 13: Comparison of Classification Results:

Model	Accuracy	Precision	Recall	F1-Score	MCC	Parameters (M)	Model-size (MB)
PCBClassNet [44]	75.33%	75.89%	75.33%	75.03%	0.7062	0.60	2.42
DInPNet[68]	78.83%	78.83%	78.83%	78.79%	0.7462	0.53	2.17
EfficientNetV2 [70][71]	80.00%	82.38%	80.00%	79.97%	0.7653	74.75	299.53
MobileNetV3 [69]	84.92%	85.76%	84.92%	85.09%	0.8199	4.20	17.02
ConvNeXt-Tiny [72][73]	84.75%	85.21%	84.75%	84.79%	0.8178	27.82	111.37

Table 14: Comparison of Class wise F1-Scores on FICS-PCB dataset[46]:

Class	Convnext_tiny [72][73]	MobileNetV3 [69]	EfficientNetV2 [70][71]	DInPNet [68]	PCBClassNet [44]
Capacitors	95.74%	95.76%	91.04%	91.23%	87.96%
Resistors	87.77%	91.82%	88.73%	84.71%	85.45%
Inductors	85.85%	86.73%	83.50%	77.97%	70.46%
Diodes	84.63%	85.01%	81.25%	83.62%	75.37%
ICs	77.57%	76.54%	65.66%	69.40%	64.14%
Transistors	77.18%	74.65%	69.62%	65.80%	66.82%
Macro Avg	84.79%	85.09%	79.97%	78.79%	75.03%
Weighted Avg	84.79%	85.09%	79.97%	78.79%	75.03%

4.6. Visual Results:

Convnext_tiny [72][73]	 True: capacitors Pred: capacitors	 True: diodes Pred: diodes	 True: resistors Pred: resistors	 True: diodes Pred: diodes	 True: ICs Pred: ICs
PCBClassNet(extracted this network from PCBSegClssNet [44])	 True: ICs Pred: ICs	 True: capacitors Pred: capacitors	 True: diodes Pred: diodes	 True: transistors Pred: transistors	 True: resistors Pred: resistors
DlnpNet [68]	 True: capacitors Pred: capacitors	 True: inductors Pred: inductors	 True: ICs Pred: transistors	 True: inductors Pred: inductors	 True: resistors Pred: resistors

EfficientNetV2 [70][71]	<p>True: capacitors Pred: capacitors</p>	<p>True: ICs Pred: transistors</p>	<p>True: capacitors Pred: capacitors</p>	<p>True: diodes Pred: diodes</p>	<p>True: inductors Pred: inductors</p>
	<p>True: inductors Pred: inductors</p>	<p>True: inductors Pred: resistors</p>	<p>True: resistors Pred: resistors</p>	<p>True: transistors Pred: transistors</p>	<p>True: transistors Pred: transistors</p>
MobileNet V3 [69]	<p>True: inductors Pred: inductors</p>	<p>True: inductors Pred: resistors</p>	<p>True: resistors Pred: resistors</p>	<p>True: transistors Pred: transistors</p>	<p>True: transistors Pred: transistors</p>
	<p>True: ICs Pred: transistors</p>	<p>True: transistors Pred: transistors</p>	<p>True: resistors Pred: resistors</p>	<p>True: capacitors Pred: resistors</p>	<p>True: transistors Pred: ICs</p>

Fig 25. Classification results on FICS-PCB [46] using 5 recent popular DL models

Sample images of failed Classifications of components observed in the classes below:

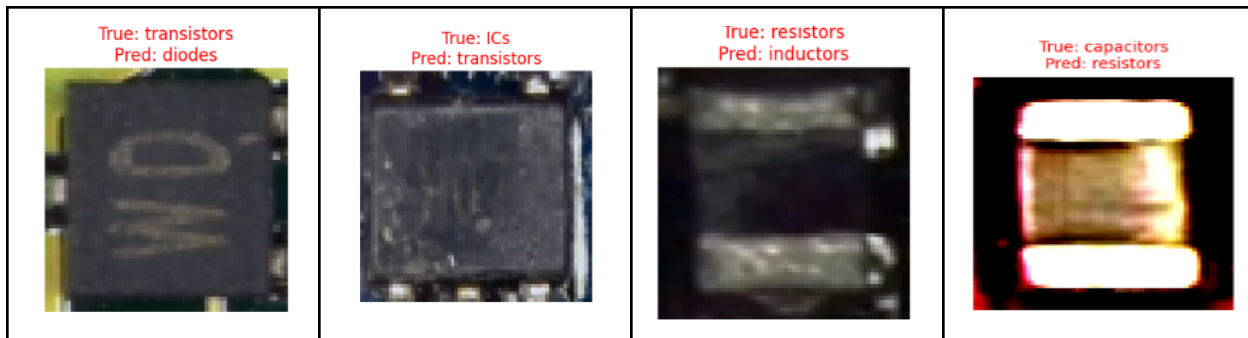


Fig 26. Sample misclassified classes

4. Challenges and Limitations

- The patch-based methodology successfully balanced high-detail retention with GPU memory limitations.
- Data augmentations significantly enhanced robustness, preparing the model for real-world imaging variations.
- Achieved strong segmentation metrics for primary component categories, laying a solid foundation for subsequent refinements and full-scale evaluations.
- Addressed severe Class imbalance problems due to rare classes and datasets such as FICS-PCB[\[46\]](#) require attention considering its variety in components and PCBs but there is scope for an approach to overcome the class imbalance severity with more loss combinations an advanced light weight model to handle large image datasets to be computationally optimal solution

CONCLUSION

In this study we experimented with many SOTA models and its performance on segmenting common components of interest such as Resistors, Capacitors, ICs and a new class Others which represent anything other than our components. Our study also experimented on new and popular classification models on the FICS-PCB dataset[46]. Throughout our work we used a patch-based deep learning approach for classification and detection of PCB components, aiming to improve the recycling of toxic materials from e-waste in the semiconductor industry. Our observation from the results convey that the Classification on the FICS-PCB[46] dataset showed high results using MobileNetV3 (84.92% accuracy, 85.09% F1) and ConvNeXt-Tiny (84.75% accuracy, 84.79% F1) experimenting on High quality images also severe class imbalance dataset such as FICS-PCB[46].

For segmentation we compared two different datasets on RGB images one being PCB-VISION[19] and other of high-resolution PCB scans on FICS-PCB[46] we tested and compared with different suitable loss functions such as Weighted CrossEntropy loss(WCCE) , DICE and Hybrid loss(WCCE+DICE), we can observe from our segmentation results that the segmentation on FICS-PCB[46] with pre-training using DeepLabV3+ with MiT-B0 (up to 89.73% Dice, 81.86% IoU) and ResNet-34 (91.20% Dice, 84.33% IoU) backbones were most effective . Also UNet++ while Unet3plus performed well it is computationally expensive and requires more training time to get better results. We have not utilised the model at full capacity of the network but with comparison the using the same environment for all models its performance is not effective compared to other Unet variants. provided balanced results across different

component classes without pre-training compared to other SOTA models despite its computational cost.

The models demonstrated robustness to diverse imaging conditions and maintained fine detail necessary for identifying small components like capacitors, resistors, and ICs through targeted data augmentation and patch-level inference. Integrating these efficient and accurate networks into recycling processes can significantly enhance the precision of automated sorting, minimizing material contamination and increasing valuable metal recovery. This research provides a resource-efficient and scalable approach for semiconductor e-waste recycling, enabling real-time robotic disassembly and promoting the circular reuse of essential electronic components.

REFERENCES

1. Serpe, A., Purchase, D., Bisschop, L., Chatterjee, D., De Gioannis, G., Garelick, H., Kumar, A., Peijnenburg, W. J. G. M., Piro, V. M. I., Cera, M., Shevah, Y., & Verbeek, S. (2025). 2002–2022: 20 years of e-waste regulation in the European Union and the worldwide trends in legislation and innovation technologies for a circular economy. *RSC Sustainability*, 3(3), 1039-1083. <https://doi.org/10.1039/D4SU00548A>
2. World Health Organization. (2024, October 1). Electronic waste (e-waste). [https://www.who.int/news-room/fact-sheets/detail/electronic-waste-\(e-waste\)](https://www.who.int/news-room/fact-sheets/detail/electronic-waste-(e-waste))
3. Mathrani, R. (2023). Challenges and innovations in achieving sustainable computing: A comprehensive analysis. *International Journal of Science and Research (IJSR)*, 12(12), 203-209. <https://doi.org/10.21275/SR231128211938>
4. Van Yken, J., Boxall, N. J., Cheng, K. Y., Nikoloski, A. N., Moheimani, N. R., & Kaksonen, A. H. (2021). E-Waste Recycling and Resource Recovery: A Review on Technologies, Barriers and Enablers with a Focus on Oceania. *Metals*, 11(8), 1313. <https://doi.org/10.3390/met11081313>
5. El-Sherif, D. M., Abouzid, M., Saber, A. N., & Hassan, G. K. (2024). A raising alarm on the current global electronic waste situation through bibliometric analysis, life cycle, and techno-economic assessment: A review. *Environmental Science and Pollution Research*, 31(28), 40778-40794. <https://doi.org/10.1007/s11356-024-33839-0>
6. Boopathi, S. (2023). A study of the printed circuit board (PCB) e-waste recycling process. In *Advances in Sustainable Practices for Industrial and Consumer Waste Management* (Chapter 9). <https://doi.org/10.4018/978-1-6684-7573-7.ch009>
7. Ruiz, A. (2024, April 15). Latest global e-waste statistics and what they tell us. The Roundup. <https://theroundup.org/global-e-waste-statistics/>
8. Kumar, A., Thorbole, A., & Gupta, R. K. (2025). Sustaining the future: Semiconductor materials and their recovery. *Materials Science in Semiconductor Processing, 185*, 108943. <https://doi.org/10.1016/j.mssp.2024.108943>
9. Bhattacharjee, J., De, A., Kamila, B. & Mandal, A. (2025). Recent scenario of e-waste recycling: chemical engineering. *International Journal of Chemical Reactor Engineering*. <https://doi.org/10.1515/ijcre-2024-0058>
10. Arbash, E., Fuchs, M., Rasti, B., Lorenz, S., Ghamisi, P., & Gloaguen, R. (2024). PCB-Vision: A multiscene RGB-hyperspectral benchmark dataset of printed circuit boards. *IEEE Sensors Journal*, PP(99), 1–1. <https://doi.org/10.1109/JSEN.2024.3380826>
11. Mohsin, M. (2024). Virtual Mines -- Component-level recycling of printed circuit boards using deep learning [Data set]. arXiv. <https://arxiv.org/abs/2406.17162>
12. Mohsin, M., Rovetta, S., Masulli, F., & Cabri, A. (2025). Automated disassembly of waste printed circuit boards: The role of edge computing and IoT. *Computers*, 14(2), 62. <https://doi.org/10.3390/computers14020062>
13. Sharma, H., & Kumar, H. (2024). A computer vision-based system for real-time component identification from waste printed circuit boards. *Journal of Environmental Management*, 351, 119779. <https://doi.org/10.1016/j.jenvman.2023.119779>
14. AdamByerly. Micro-pcb Images Dataset. 2021. Available online: <https://www.kaggle.com/datasets/frettapper/micropcb-images> (accessed 1 December 2022)

15. Glučina, M., Andelić, N., Lorencin, I., & Car, Z. (2023). Detection and classification of printed circuit boards using YOLO algorithm. *Electronics*, 12(667). <https://doi.org/10.3390/electronics12030667>
16. Khan, A. (2024). A triad of approaches for PCB component segmentation and classification using U-Net, SAM, and Detectron2 [Master's thesis, University of Kansas].
17. Shen, M., Liu, Y., Chen, J., Ye, K., Gao, H., Che, J., Wang, Q., He, H., Liu, J., Wang, Y., & Jiang, Y. (2024). Defect detection of printed circuit board assembly based on YOLOv5. *Scientific Reports*, 14, 70176. <https://doi.org/10.1038/s41598-024-70176-1>
18. Ding, R., Dai, L., Li, G., & Liu, H. (2019). TDD-Net: A tiny defect detection network for printed circuit boards. *CAAI Transactions on Intelligence Technology*, 4(2). <https://doi.org/10.1049/trit.2019.0019>
19. Arbash, Elias, Fuchs, Margret, Rasti, Behnoor, Lorenz, Sandra, Ghamisi, Pedram, & Gloaguen, Richard. (2024). PCB-Vision: A Multiscene RGB-Hyperspectral Benchmark Dataset of Printed Circuit Boards (Version 1) [Data set]. Rodare. <http://doi.org/10.14278/rodare.2704>
20. Pasunuri, A., Jessurun, N., Dizon-Paradis, O. P., & Asadizanjani, N. (2021). A comparison of neural networks for PCB component segmentation. 2021 IEEE International Symposium on Hardware Oriented Security and Trust (HOST), Tysons Corner, VA, USA, 113-123. <https://doi.org/10.1109/HOST49136.2021.9702286>
21. Cabrera, R. (2019). Electronic devices and circuits. Scientific e-Resources. Retrieved from <https://books.google.com>
22. Chalana, A., Singh, K., Sharma, S., Bhardwaj, V., Rai, R.K. (2023). E-waste Management: Prospects and Strategies. In: Debbarma, P., Kumar, S., Suyal, D.C., Soni, R. (eds) Microbial Technology for Sustainable E-waste Management. Springer, Cham. https://doi.org/10.1007/978-3-031-25678-3_19
23. Jha, H., Upakrishnam, S., & Dubey, B. (2024). Recovery of precious metals and rare earth elements from e-waste. In Environmental sustainability and waste management (Chapter 19). CRC Press. <https://doi.org/10.1201/9781003327646-19>
24. Pourya, Z., Mehran, A., Elaheh, H., & Mohammad Amin, A. (2023). A review study on a polymer optical nanosensor named "Pourya-Zar Sensor" for detection of Cu heavy metal ions in aquatic environments. *Recent Advances in Petrochemical Science*, 7(5), 555724. <https://doi.org/10.19080/RAPSCI.2023.07.555724>
25. Omundi, E. A., Ndiba, P. K., & Koech, G. C. (2022). Complexity of e-waste and its management challenges in developing countries—A review. *International Journal of Environmental Sciences and Natural Resources*, 31(2), 1-17. <https://doi.org/10.19080/IJESNR.2022.31.556309>
26. Abdelbasir, S. M., & Kamel, A. H. (2018). Status of electronic waste recycling techniques: A review. *Environmental Science and Pollution Research*, 25(4). <https://doi.org/10.1007/s11356-018-2136-6>
27. Patwa, J., Sharma, A., & Flora, S. J. S. (2022). Chapter 29 - Arsenic, cadmium, and lead. In R. C. Gupta (Ed.), Reproductive and Developmental Toxicology (Third Edition) (pp. 547-571). Academic Press. <https://doi.org/10.1016/B978-0-323-89773-0.00029-1>
28. Nyeko, S. J., Mlay, S. V., Amerit, B., Abima, B., Among, J., Nyero, A. I., Odiya, J., & Ogen, C. (2023). The impact of electronic-electrical waste on human health and

- environment: A systematic literature review. *Journal of Engineering and Technology Research, 15*(1), 1-16. <https://doi.org/10.5897/JETR2021.0726>
29. Charitopoulou, M.A., Kalogiannis, K.G., Lappas, A.A. et al. Novel trends in the thermo-chemical recycling of plastics from WEEE containing brominated flame retardants. Environ Sci Pollut Res 28, 59190–59213 (2021). <https://doi.org/10.1007/s11356-020-09932-5>
 30. Leung, A. O. W. (2019). Chapter 15 - Environmental contamination and health effects due to e-waste recycling. In Electronic Waste Management and Treatment Technology (pp. 335-362). <https://doi.org/10.1016/B978-0-12-816190-6.00015-7>
 31. Barrueto, Y., Hernández, P., Jiménez, Y. P., & Morales, J. (2022). Properties and application of ionic liquids in leaching base/precious metals from e-waste: A review. Hydrometallurgy, 212, 105895. <https://doi.org/10.1016/j.hydromet.2022.105895>
 32. Li, X., Wu, Y., & Tan, Z. (2022). An overview on bioremediation technologies for soil pollution in e-waste dismantling areas. Journal of Environmental Chemical Engineering, 10(3), 107839. <https://doi.org/10.1016/j.jece.2022.107839>
 33. Zhu, Y., Li, B., Wei, Y., Zhou, S., & Wang, H. (2023). Recycling potential of waste printed circuit boards using pyrolysis: Status quo and perspectives. Process Safety and Environmental Protection, 173, 437–451. <https://doi.org/10.1016/j.psep.2023.03.018>
 34. Wang, K. (2023). Advances in e-waste recycling: Physical and chemical treatment methods. Highlights in Science, Engineering and Technology, 73, 378–383. <https://doi.org/10.54097/hset.v73i.13106>
 35. Laszlo, R., Holonec, R., Copîndean, R., & Dragan, F. (2019, May). Sorting system for e-waste recycling using contour vision sensors. In 2019 8th International Conference on Modern Power Systems (MPS) (pp. 1–4). IEEE. <https://doi.org/10.1109/MPS.2019.8759739>
 36. Ashiq, A., Kulkarni, J., & Vithanage, M. (2019). Hydrometallurgical recovery of metals from e-waste. In M. N. V. Prasad & M. Vithanage (Eds.), Electronic waste management and treatment technology (pp. 225–246). Butterworth-Heinemann. <https://doi.org/10.1016/B978-0-12-816190-6.00010-8>
 37. Narayanasamy, M., Dhanasekaran, D., & Thajuddin, N. (2021). Bioremediation of noxious metals from e-waste printed circuit boards by Frankia. Microbiological Research, 245, 126707. <https://doi.org/10.1016/j.micres.2021.126707>
 38. Yu, H., Ma, J., Chen, F., Zhang, Q., Wang, Y., & Bian, Z. (2022). Effective remediation of electronic waste contaminated soil by the combination of metal immobilization and phytoremediation. Journal of Environmental Chemical Engineering, 10(3), 107410. <https://doi.org/10.1016/j.jece.2022.107410>
 39. Faraji, F., Golmohammadzadeh, R., & Pickles, C. A. (2022). Potential and current practices of recycling waste printed circuit boards: A review of the recent progress in pyrometallurgy. Journal of Environmental Management, 316, 115242. <https://doi.org/10.1016/j.jenvman.2022.115242>
 40. Oke, E.A., Potgieter, H. Discarded e-waste/printed circuit boards: a review of their recent methods of disassembly, sorting and environmental implications. J Mater Cycles Waste Manag 26, 1277–1293 (2024). <https://doi.org/10.1007/s10163-024-01917-7>
 41. López, M., Reche, C., Pérez-Albaladejo, E., Porte, C., Balasch, A., Monfort, E., Eljarrat, E., & Viana, M. (2022). E-waste dismantling as a source of personal exposure and

- environmental release of fine and ultrafine particles. *Science of The Total Environment*, 833, 154871. <https://doi.org/10.1016/j.scitotenv.2022.154871>
42. Jessurun, N., Dizon-Paradis, O. P., Harrison, J., Ghosh, S., Tehranipoor, M. M., Woodard, D. L., & Asadizanjani, N. (2023). FPIC: A novel semantic dataset for optical PCB assurance. arXiv preprint arXiv:2202.08414. <https://doi.org/10.48550/arXiv.2202.08414>
 43. Liu, L., Ke, C., & Lin, H. (2023). Mobile-Deep Based PCB Image Segmentation Algorithm Research. *Computers, Materials & Continua*, 77(2), 2443–2461. <https://doi.org/10.32604/cmc.2023.042582>
 44. Makwana, D., Teja, S. C. R., & Mittal, S. (2022). Pcbsegclassnet - A Light-Weight Network for Segmentation and Classification of PCB Component. *SSRN Electronic Journal*. <https://doi.org/10.2139/ssrn.4241188>
 45. Jessurun, N., Dizon-Paradis, O. P., Harrison, J., Ghosh, S., Tehranipoor, M. M., Woodard, D. L., & Asadizanjani, N. (2022). FPIC: A Novel Semantic Dataset for Optical PCB Assurance. <https://arxiv.org/abs/2202.08414>
 46. Lu, H., Mehta, D., Paradis, O., Asadizanjani, N., Tehranipoor, M., & Woodard, D. L. (2020). *FICS-PCB: A Multi-Modal Image Dataset for Automated Printed Circuit Board Visual Inspection* [Preprint]. Florida Institute for Cybersecurity (FICS) Research. Available at: <https://www.researchgate.net/publication/342757891>
 47. Huang, W., & Wei, P. (2019). *A PCB Dataset for Defects Detection and Classification* [Preprint]. arXiv. <https://arxiv.org/abs/1901.08204>
 48. Tang, S., He, F., Huang, X., & Yang, J. (2019). *Online PCB Defect Detector on a New PCB Defect Dataset* [Preprint]. arXiv. <https://arxiv.org/abs/1902.06197>
 49. Mahalingam, G., Marshall Gay, K., & Ricanek, K. (2019). *PCB-METAL: A PCB Image Dataset for Advanced Computer Vision Machine Learning Component Analysis*. In Proceedings of the 2019 16th International Conference on Machine Vision Applications (MVA). <https://doi.org/10.23919/MVA.2019.8757928>
 50. Pramerdorfer, C., & Kampel, M. (2015). *A Dataset for Computer-Vision-Based PCB Analysis*. In Proceedings of the 2015 Machine Vision Applications (MVA) Conference. <https://doi.org/10.1109/MVA.2015.7153209>
 51. Kuo, C.-W., Ashmore, J., Huggins, D., & Kira, Z. (2019). Data-efficient graph embedding learning for PCB component detection. *arXiv*. <https://arxiv.org/abs/1811.06994>
 52. Ronneberger, O., Fischer, P., & Brox, T. (2015). *U-Net: Convolutional networks for biomedical image segmentation*. arXiv preprint arXiv:1505.04597. Available at <https://arxiv.org/abs/1505.04597>.
 53. Persson, A. (2021). *Semantic segmentation using U-Net*. Retrieved from https://github.com/aladdinpersson/Machine-Learning-Collection/blob/master/ML/Pytorch/image_segmentation/semantic_segmentation_unet/model.py.
 54. Oktay, O., Schlemper, J., Folgoc, L. L., Lee, M., Heinrich, M., Kainz, B., ... Rueckert, D. (2018). *Attention U-Net: Learning where to look for the pancreas*. arXiv preprint arXiv:1804.03999. Available at <https://arxiv.org/abs/1804.03999>.
 55. Lee, J. (n.d.). *Adapted binary segmentation model AttUnet architecture to multiclass segmentation*. Retrieved from

https://github.com/LeeJunHyun/Image_Segmentation/blob/master/network.py.

56. Zhang, C., Wei, Y., Zhang, Y., & Yang, Q. (2017). *Road extraction by deep residual U-Net*. arXiv preprint arXiv:1711.10684. Available at <https://arxiv.org/pdf/1711.10684.pdf>.
57. Rishikksh20. (n.d.). *Adapted binary segmentation model ResUnet architecture to multiclass segmentation*. Retrieved from https://github.com/rishikksh20/ResUnet/blob/master/core/res_unet.py.
58. Milesial. (n.d.). Pytorch-UNet. Retrieved from <https://github.com/milesial/Pytorch-UNet>.
59. YZY-stack. (n.d.). *UNet-MobileNet-Pytorch*. Retrieved from <https://github.com/YZY-stack/UNet-MobileNet-Pytorch/tree/main>.
60. Huang, H., Lin, L., Tong, R., Hu, H., Zhang, Q., Iwamoto, Y., Han, X., Chen, Y.-W., & Wu, J. (2020). *UNet 3+: A full-scale connected UNet for medical image segmentation*. arXiv. <https://arxiv.org/abs/2004.08790>.
61. Russel0719. (n.d.). *UNet-3-Plus-Pytorch*. GitHub. Retrieved May 7, 2025, from <https://github.com/russel0719/UNet-3-Plus-Pytorch>.
62. qubvel-org. (n.d.). *Segmentation Models PyTorch*. GitHub. Retrieved May 7, 2025, from https://github.com/qubvel/segmentation_models.pytorch.
63. VainF. (n.d.). *DeepLabV3Plus-Pytorch*. GitHub. Retrieved May 7, 2025, from <https://github.com/VainF/DeepLabV3Plus-Pytorch>.
64. Albumentations. (n.d.). *PyTorch Transforms API Reference*. Retrieved May 7, 2025, from <https://albumentations.ai/docs/api-reference/pytorch/transforms/>.
65. PyTorch. (n.d.). *torch.nn.CrossEntropyLoss documentation*. Retrieved May 7, 2025, from <https://docs.pytorch.org/docs/stable/generated/torch.nn.CrossEntropyLoss.html>.
66. qubvel. (n.d.). *Segmentation Models - Losses*. GitHub. Retrieved May 7, 2025, from https://github.com/qubvel/segmentation_models/blob/master/segmentation_models/losses.py.
67. Scikit-learn. (n.d.). *sklearn.metrics.confusion_matrix documentation*. Retrieved May 7, 2025, from https://scikit-learn.org/stable/modules/generated/sklearn.metrics.confusion_matrix.html.
68. Mantravadi, A., Makwana, D., R, S. C. T., & Singhal, R. (2023). *Dilated Involutional Pyramid Network (DInPNet): A novel model for printed circuit board (PCB) components classification*. 24th International Symposium on Quality Electronic Design (ISQED'23), California, USA. <https://doi.org/10.1109/ISQED57927.2023.10129388>.
69. Howard, A., Sandler, M., Chu, G., Chen, L.-C., Chen, B., Tan, M., Wang, W., Zhu, Y., Pang, R., Vasudevan, V., Le, Q. V., & Adam, H. (2019). *Searching for MobileNetV3*. arXiv. Retrieved May 7, 2025, from <https://arxiv.org/pdf/1905.02244>.
70. Balawejder, M. (n.d.). *EfficientNetV2 -Deep Learning Collection*. GitHub. Retrieved from <https://github.com/maciejbalawejder/Deep-Learning-Collection/blob/main/ConvNets/EfficientNetV2/readme.md>.
71. Tan, M., & Le, Q. V. (2021). *EfficientNetV2: Smaller models and faster training*. arXiv. Retrieved May 7, 2025, from <https://arxiv.org/abs/2104.00298>.
72. Zhang, Y., Xu, A., Lan, D., & Goh, H. H. (2022). *ConvNeXt-based anchor-free object detection model for infrared image of power equipment*. Energy Reports, 9(2). <https://doi.org/10.1016/j.egyr.2023.04.145>.

73. Liu, Z., Mao, H., Wu, C.-Y., Feichtenhofer, C., Darrell, T., & Xie, S. (2022). *A ConvNet for the 2020s*. arXiv. Retrieved May 7, 2025, from <https://arxiv.org/abs/2201.03545>.
74. Zhou, Z., Siddiquee, M. M. R., Tajbakhsh, N., & Liang, J. (2018). *UNet++: A nested U-Net architecture for medical image segmentation*. arXiv. Retrieved May 7, 2025, from <https://arxiv.org/abs/1807.10165>.
75. Zhoudaxia233. (n.d.). *PyTorch-Unet*. GitHub. Retrieved May 7, 2025, from <https://github.com/zhoudaxia233/PyTorch-Unet>.
76. Wang, Z., Berman, M., Rannen-Triki, A., Torr, P. H. S., Tuia, D., Tuytelaars, T., Van Gool, L., Yu, J., & Blaschko, M. B. (2023). *Revisiting evaluation metrics for semantic segmentation: Optimization and evaluation of fine-grained intersection over union*. arXiv. <https://arxiv.org/abs/2310.19252>
77. Changqian Yu et.al.(2020). BiSeNet V2: Bilateral network with guided aggregation for real-time semantic segmentation. *arXiv preprint arXiv:2004.02147*. Retrieved from <https://arxiv.org/abs/2004.02147>
78. Zh320. (2023). Real-time semantic segmentation in PyTorch. Retrieved from <https://github.com/zh320/realtimsemantic-segmentation-pyt>
79. Fan, M., Lai, S., Huang, J., Wei, X., Chai, Z., Luo, J., & Wei, X. (2021). Rethinking BiSeNet for real-time semantic segmentation. *arXiv preprint arXiv:2104.13188*. Retrieved from <https://arxiv.org/abs/2104.13188v1>
80. Sun, L., Wang, Z., Xu, X., & Zhao, H. (2021). Deep dual-resolution networks for real-time and accurate semantic segmentation of road scenes. *arXiv preprint arXiv:2101.06085*. Retrieved from <https://arxiv.org/abs/2101.06085>